Check for updates

Preventing acute lung injury from progressing to pulmonary fibrosis by maintaining ERS homeostasis through a multistage targeting nanomicelle

Lihua Luo [a,1], Zhenyu Luo [a,1], Junlei Zhang [a], Xu Liu [a], Jiaxin Huang [a], Sijie Wang [a], Hang Yin [a], Xuemeng Guo [a], Yilong Hu [a], Yichao Lu [a], Xinyu Shan [a], Huihui Liu [a], Yingying Shi [a], Yongzhong Du [a], Fuchun Yang [b,*], Jian You [a,*]

[a] College of Pharmaceutical Sciences, Zhejiang University, NO. 866 Yuhangtang Road, Hangzhou, Zhejiang 310058, China
[b] Department of Hepatobiliary and Pancreatic Surgery, The First Affiliated Hospital, Zhejiang University School of Medicine, Hangzhou 310003, Zhejiang Province, China

ARTICLE INFO

ABSTRACT

Acute lung injury / acute respiratory distress syndrome (ALI/ARDS) or pulmonary fibrosis (PF) has been regarded as a global health issue with high mortality and limited drug therapy. Clinical evidence suggests that undesired macrophage polarization (M) is the main factor driving the development of ALI/ARDS, and endoplasmic reticulum stress (ERS) has been considered an important determinant of M polarization. Accordingly, we proposed a hypothesis that restoration of ER homeostasis would effectively balance the homeostasis of M and prevent ALI from progressing to pulmonary fibrosis (PF). To this end, we designed a multistage targeted nanomicelle mainly based on hyaluronic acid (HA) and α-tocopherol succinate (α-TOS) (named as HSST or pHSST with peptide modified) to load ERS inhibitor (KIRA6, K) and anti-inflammatory drug (Dexamethasone, Dex) respectively. When inflammation occurred, K-loaded pHSST (K@pHSST) and Dex-loaded HSST (Dex@HSST) firstly achieved lung targeting by "hitchhiking" myeloid M and neutrophils (Neu) that patrol in the blood and then achieved inflammation-associated cells targeting through a CD44 receptor-ligand-mediated mode by HA. For K@pHSST, at the same time, the ER-targeting molecule (Pardaxin, Par) was used to modify the nanomicelles for tertiary ER-targeting effect and specifically delivering of the K to ER. While in response to high-level intracellular reactive oxygen species (ROS), Dex@HSST disintegrated due to the reductive α-tocopherol succinate (α-TOS) and disulfide bond. The released Dex exerted anti-inflammatory effects and promoted type 2 M cells (M2) polarization via activating intracellular glucocorticoid receptors. Through the combined administration of Dex@HSST and K@pHSST, this strategy could effectively reduce ROS, limit cytokine storm, restore ER homeostasis, reverse imbalanced M polarization, and fundamentally resolve ALI and prevent PF.

© 2022 Elsevier Ltd. All rights reserved.

Introduction

Acute lung injury or acute respiratory distress syndrome (ALI/ARDS) is a common cause of respiratory failure in patients with severe pneumonia, which may lead to irreversible lung damage and even death[1–3]. Clinical evidence now suggests that imbalanced polarization of macrophage (M) is a major driver for pulmonary fibrosis (PF)[4]. As a devastating disease with different pathological stages, PF includes the "exudative phase", "recovery phase" and "fibrotic phase". The exudative phase is mainly mediated by type-1 M cells (M1). If excessive inflammation in this period is not completely relieved, PF will progress to a state of chronic inflammation. On the other hand, under long-term inflammation, type-2 M cells (M2) will hyperpolarize to cause PF "repair phase" disorder and eventually promote the pathogenesis of fibrosis[5–8].

Research evidence suggests that excessive endoplasmic reticulum stress (ERS)- associated with M-cell hyperpolarization plays an important role in the initiation and development of PF [9–11]. During the "exudative phase", inflammatory pathogens cause ER
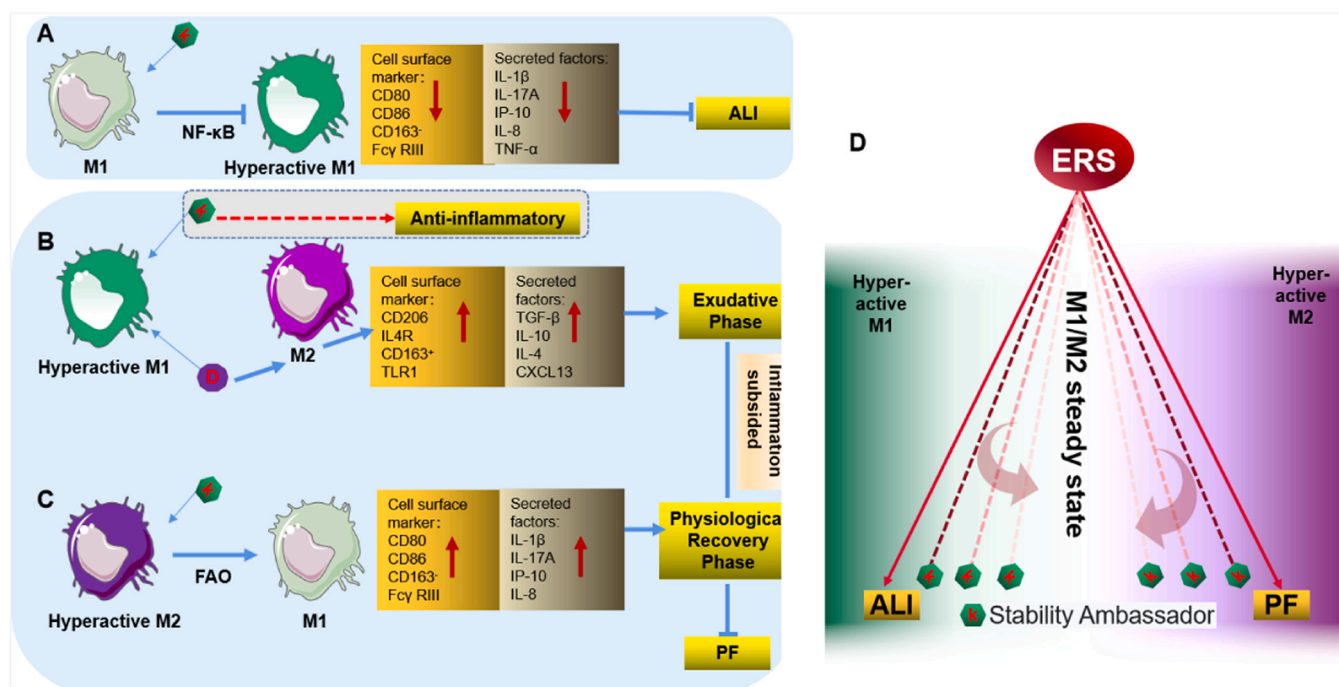
Scheme 1. The mechanism of K and Dex in preventing ALI from progressing to PF. (A) Inhibiting the excessive ERS of hyperactive M1 cells with K can decrease its phenotype markers and reduce the inflammatory factors through the NF-κB pathway and then play the function of anti-ALI. **(B)** The anti-inflammation mechanism of K and Dex in the exudative phase of PF. **(C)** In the recovery phase of PF, K repolarizes M2 to M1 by interfering with the FAO metabolism of M2. **(D)** K is regarded as a "stability ambassador" during ALI and PF contributing to M1/M2 state steady.

misfolding and unfolded protein response (UPR) of M cells with concomitant activation of phosphorylated protein kinase (pAKT), kappa B kinase (IKK), and nuclear factor kappa-B (IκB) inhibitors as well as NF-κB signaling pathway, which mediate the malignant inflammation and M1 hyperpolarization[12]. In addition, the excessive ERS also promotes M1 development by downregulating dual specificity phosphatase 1 (Dusp1) and enhancing the activation of c-Jun N-terminal kinase (JNK) [13,14]. The resultant pro-inflammatory cytokines and high levels of reactive oxygen species (ROS) induce a cytokine storm that may lead to a phase of the self-repairing disorder. Meanwhile, ERS without restoration of homeostasis promotes the polarization of M2 type by regulating several important pathways including c-Jun N-terminal kinase-peroxisome proliferator-activated receptor γ (JNK-PPARγ) signal transducer and activator of transcription 6-krüppel-like factor 4 (STAT6-KLF4), leading to the apoptosis of alveolar epithelial cell and the activation of fibroblast[15,16].

Accordingly, a hypothesis was proposed in this study that restoration of ERS homeostasis combined with glucocorticoid receptor agonists, Dexamethasone (Dex) was considered as the optimal medication for ALI/ARDS in much research evidence. When combined with GRs, a low dosage of Dex can play a pro-inflammatory role by antagonizing NF-κB, enhancing the number of polarized M2 cells, and accelerating the resolution of lung inflammation and edema, which would effectively balance the polarization of M1/M2. Therefore, it may be the most suitable model drug in this study to prevent the progression of ALI/ARDS to PF from the perspective of ERS [17–19]. Inositol-requiring enzyme 1α / X-box binding protein 1 (IRE1α/Xbp1) axis is involved in pro-inflammatory responses during adaptive UPR and is thought to be a perpetuating factor of inflammation in various chronic diseases[20–23]. What's more, appropriate activation of the IRE1α/Xbp1 axis restores ER homeostasis by driving the polarization of M cells through the production of various ER chaperones[24]. Therefore, specific inhibition of the

hyperactivated IRE1α/Xbp1 pathway with KIRA6 (K) will benefit ER homeostasis and M1/M2 polarization.

In detail, by inhibiting the M1-excessive ERS with K, the phenotype markers and inflammation factors of hyperactive M1 cells will be reduced. Thus, effectively exerting its anti-ALI or anti-inflammatory effects **(Scheme1 A and B)**. Although inhibition of IRE1-α/XBP-1 in M1 cells can not directly promote M2 polarization[12,25], the anti-inflammatory effect of K is amplified by reducing the M1/M2 ratio. Dex, on the other hand, is conducive to the polarization of hyperactive M1 to M2 cells, which can promote the up-regulation of M2 phenotype markers and the release of anti-inflammatory factors to eliminate inflammation in the exudative phase of PF [26,27] **(Scheme 1 B)**. Afterward, in the hyperactive M2-dominated repair phase, inhibition of IRE1-α/XBP-1 with K can re-polarize hyperactive M2 to M1 cells by affecting their fatty acid oxidation (FAO) metabolic pathway[13,28], and then alleviate PF progression **(Scheme C)**.

In a word, K applied here acts as a stability ambassador for ERS homeostatic reparation which benefits the storage of balanced M1/M2 polarization during the PF disease. In the exudative phase (or ALI model), by inhibiting the NF-κB pathway, etc., K can effectively reverse the hyperactivation of M1 cells and anti-inflammatory. Meanwhile, in the recovery phase of PF, in which M2 is hyperactivated, K can repolarize M2 to M1 by interfering with the FAO metabolism of M2 **(Scheme D)**. M1/M2 polarization homeostasis is then achieved with the help of K.

So far, although effective treatments for ALI/ARDS or PF have not been found[1,29], nanomedicine with precise targeting and synergistic effect now has been regarded as a promising strategy to prevent ALI from progressing to PF [30,31]. Here, a multi-functional nanomicelle is designed with hyaluronic acid (HA) and reduced D-alpha-tocopheryl succinate (α-TOS). Being linked through ROS-responsive disulfide bond (-SS-), HA-SS-α-TOS copolymer is formed, followed by the preparation of nanomicelles with self-assembled nanoprecipitation, named HSST, which could be enriched into inflamed lung tissue, enabling primary lung targeting effect by

hitchhiking M and Neu (Scheme 2A) [32–35]. Meanwhile, it can specifically recognize the CD44 receptor that is upregulated on the surface of damaged bronchial epithelial cells as well as inflammatory M cells (secondary cellular targeting effect) and make it possible for Dex-loaded HSST (Dex@HSST) to release drug intracellularly (Scheme 2B) [36–38]. To make K precisely work on the ER of M cells, the ER-targeting molecule pardaxin (Par) [39–42] is used to modify the K-loaded HSST (K@pHSST), which can dramatically enhance the therapeutic efficacy of K, restore the M-cell ER homeostasis, and eliminate the M1-mediated inflammation (Scheme 2C).

In all, with the combination of Dex@HSST and K@pHSST, our strategy successfully reduced the level of ROS and cytokine storm (Scheme 2D), reversed imbalanced M polarization by restoring ER homeostasis, fundamentally overcame ALI/ARDS, prevented PF (Scheme 2E).

Results

1. Fabrication of K@pHSST and Dex@HSST

The nanomicelle was constructed as previously shown[43,44]. Redox-sensitive cystamine (CYS)-conjugated hyaluronic acid (HA-CYS) was first synthesized by amine-reactive coupling. Then, the carboxyl group on α-TOS was activated by EDC and N-hydroxysuccinimide (NHS), followed by coupling with the amino group on HA–CYS to form the amphiphilic polymer HSST, which could disperse in water and form nanomicelles by self-aggregation. ER-targeted molecule (DSPE-PEG-Par[39,45]) and hydrophobic drugs K or Dex were loaded into the hydrophobic core of HSST by solvent volatilization (Fig. S1). The fabricated nanomicelles were named HSST, K@HSST, and Dex@HSST (i.e., blank nanomicelle, and nanomicelle containing K or Dex respectively). K@pHSST and pHSST were ER-targeted nanomicelles with or without loading K. The spherical morphology of these nanomicelles was confirmed by transmission electron microscopy (TEM) (Fig. 1A). The sizes of the four kinds of nanomicelles were approximately 150 nm and uniformly distributed as determined by dynamic light scattering. Comparatively speaking, the drug loading-nanomicelles became more round in shape and had a smaller PDI (Fig. 1A, B). Yet, the introduction of ER-targeting molecules did not change the size and shape of the micelles. The surface zeta potentials of the nanomicelles were around − 30 mV (Fig. 1C). Encapsulation efficiency (EE) of K and Dex in pHSST or HSST, as calculated by comparing the amount in the micelles to the feeding amount of the drug, was over 80% w/w (Fig. 1D). The drug release behavior of K@pHSST and Dex@HSST in various ROS conditions was detected. As shown in Fig. 1E and Fig. 1F, in the absence of H_2O_2 (pH 7.4), only ~50% quantity of K or Dex was released from the nanomicelles within 48 h, demonstrating good stability in normal conditions, which may prevent the side effects caused by accidental drug release in normal tissues. When the H_2O_2 increased to 10 mM, over 80% of the drugs were released, displaying a favorable inflammatory response. As HA could specifically recognize CD44 receptors, which was regarded as an adhesion molecule that is upregulated on the surface of M and Neu cells (Fig. S2), we then investigated the uptake capacity of different nanomicelles by M cells. It was found that pHSST was easier to be taken up by M cells due to the membrane-penetrating effect of Par, and the inflammatory-activated M1 cells had a stronger uptake capacity for nanomicelles (Fig. 1G and H). Similar experimental results were also verified in inactive Neu (N0) and active Neu (N1) cells (Fig. S3). According to our previous study, the Par could mediate nanoparticles internalized into the ER of cells through a caveolin-mediated endocytic pathway [39]. Confocal images in Fig. 1I and J displayed that pHSST was mostly located in the ER, while HSST was hardly co-located with ER. And there was no significant difference in the efficiency of ER localization with or without the activation of M cells.

2. pHSST selectively accumulated in inflamed lung tissue via hitchhiking M and Neu cells

M and Neu cells were activated during inflammation in response to numerous pro-inflammatory cytokines produced by immune cells, and then, recruited to the inflamed tissue. While activation, M and Neu cells highly expressed CD44 adhesion receptors and upregulated their phagocytic ability[46]. Through specific recognition with the CD44 receptor, pHSST was phagocytosed by the circulating M and Neu cells after i.v. administration, and then enriched in the inflamed lung tissue in the form of a hitchhiker (Fig. 2A). Lung immunofluorescence sections from ALI model mice displayed higher expression of CD44 protein surrounding the lung alveolus, as well as the more infiltrated M (CD68 +) cells, compared with that of the sham-operated (SO) mice. Moreover, there were a large number of myeloperoxidase (MPO) signals around the alveolus of ALI mice, indicating that inflammation was accompanied by the recruitment of a large number of Neu cells (Fig. 2B-E).

Mice were injected with DIR-labeled micelles (DIR-HSST and DIR-pHSST). Six hours later, it was found that the accumulation of DIR-HSST and DIR-pHSST in the lungs of ALI model mice was enhanced significantly different from that in SO mice of both BALB/C and C57 strains (Fig. 2F). We also found that Par-modified nanomicelles could specifically enrich in lung tissues while reducing their accumulation in the liver (Fig. S4 and Fig. 2G). For the liver removal and lung tissue off-target efficiency of the nanomicelles, we quantified the distribution of nanomicelles into mice for 24 h in each organ, concerning the fluorescence of the injected volume, and concluded that the highest percentage of pHSST accumulated in the lungs of ALI, which was about 7-fold higher compared to healthy mice (Fig. S5).

We speculated that the cationic transmembrane effect of Par promoted the hitchhiking effect in vivo, which might enhance the uptake of the nanomicelles by M and Neu cells. Fig. 2 H-I and Fig. S4 and Fig. S5 showed that pHSST injected into ALI mice mainly accumulated around the alveolus, whereas both CD44 and CD68 were highly expressed, while the fluorescent signals of pHSST, CD44, and CD68 were very weak around the alveolus of SO mice.

Phagocytosed by Neu cells in vivo, pHSST could be carried to the inflammatory lung. From Fig. S6, it could be seen that the MPO and pHSST signals around the alveolus of ALI model mice were stronger than those in the SO mouse. The signals of CD44, CD68, and MPO have mostly clustered around the alveolus, which further proved that the lung targeting of pHSST was mediated by the CD44 receptor and displayed inflammatory (M, Neu) cell tropisms.

To further verify that pHSST was enriched in the lung tissue also by hitchhiking M cells, FITC-labeled ER-targeting micelles (FITC-pHSST) were prepared and M cells in mice were then depleted by chlorophosphonic acid liposomes (CaL) (Fig. S7). For ALI model mice in the WT group (without M cell depletion), FITC-pHSST displayed a very obvious accumulation in the lung tissue, while it was mainly distributed in the liver, kidney, spleen, and heart in the SO mice, which further indicated that pHSST has the ability of inflammatory targeting. In the CaL-treated mice (M cells were depleted), a high leveled accumulation of pHSST in the lungs of ALI model mice can still be found, while for SO mice, the accumulation of pHSST in the inflamed lungs was significantly reduced, because the depletion of M cells reduced the hitchhiking effect of pHSST, and the lung enrichment of pHSST was mainly mediated by Neu cells and the highly expressed CD44 in the alveolar epithelium (Fig. S8). After adoptive FITC-pHSST swallowed M1 cells (FITC-pHSST@DIR-M1) into the CaL-treated mice, no significant difference in pHSST enrichment in the lung was observed between ALI and SO mice, indicating that re-infusion of activated M cells complemented its accumulation in the inflamed lung (Fig. 2J-K).

Immunofluorescence staining of lung sections also showed a clear trend of inflammatory accumulation of infused M1 cells
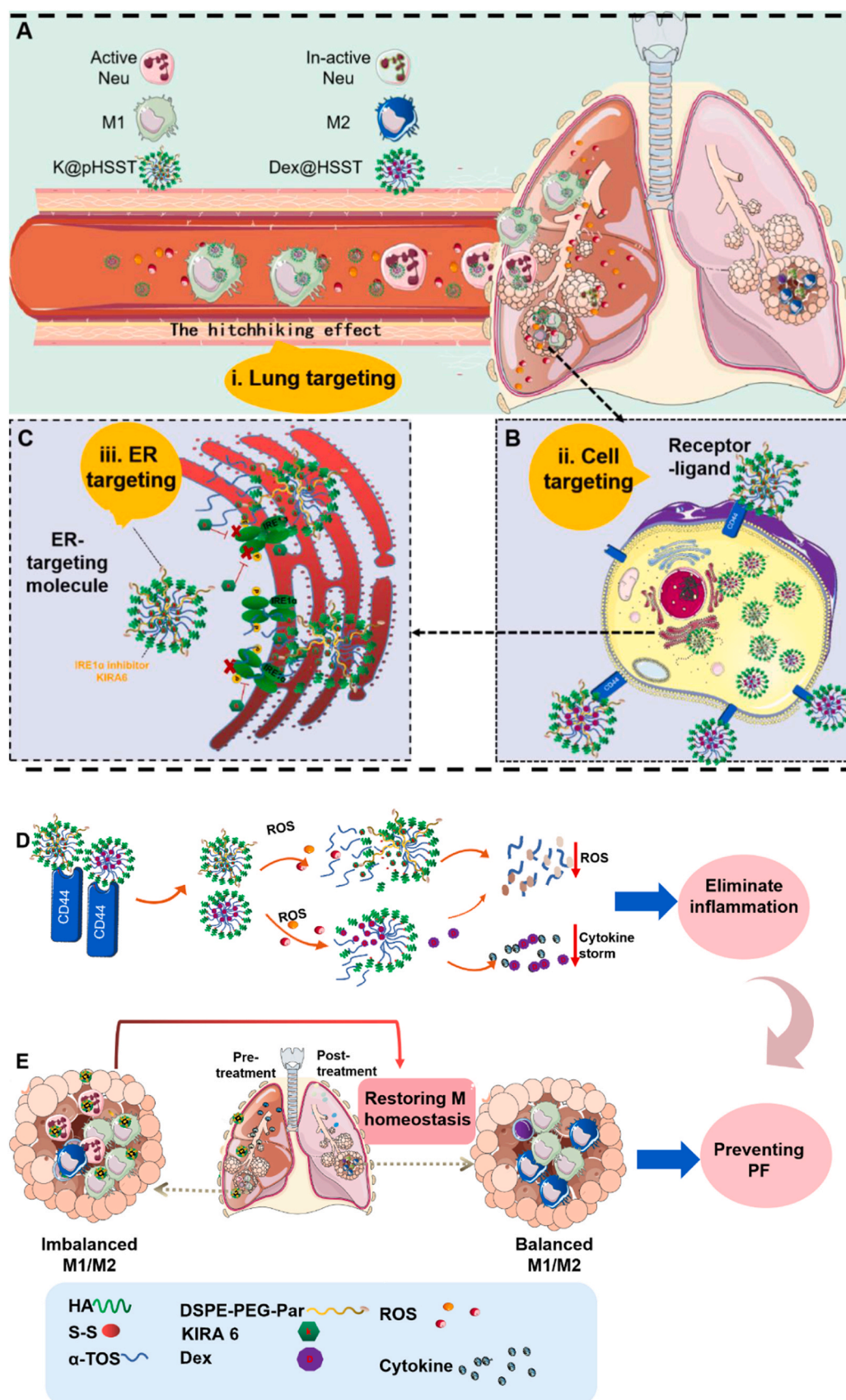
Scheme 2. The schematic diagram of the nanomicelles in preventing ALI from progressing to pulmonary fibrosis. (A-C) The mechanism of step-wised targeting. Primary lung tissue targeting effect through the "hitchhiking effect" by M and Neu (A). Secondary cellular targeting effect mediated by CD44 receptor upregulated on the surface of in-flammatory M and Neu cells (B). Tertiary ER targeting is mediated by the ER-targeting molecule pardaxin (C). **(D)** The step-wised targeting nanomicelles loaded with K or Dex can specifically recognize CD44 receptors, and disintegrate in response to high intracellular ROS, release drugs, eliminate cytokine storms, and effectively anti-ALI. **(E)** Progression from ALI to PF is reversed by remodeling M cell homeostasis through a precise restoration of ER with K.
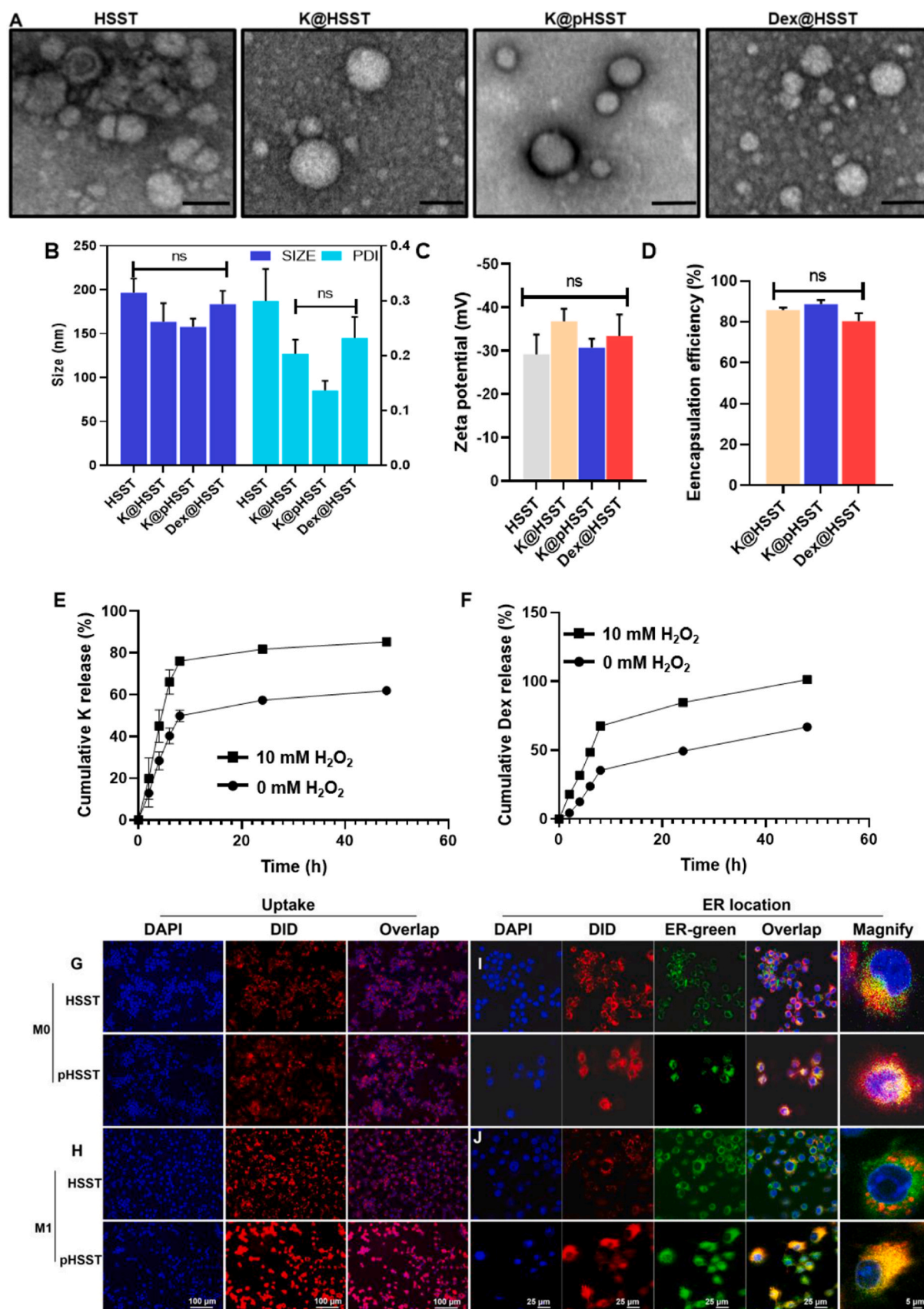
Fig. 1. Fabrication of the ER-targeted pHSST. (A-C) Transmission electron micrographs, scare bar: 200 nm (A), size distribution (B), and surface zeta potential (C) of HSST, K@HSST, K@pHSST, and Dex@HSST. (D) The drug encapsulation efficiency. **(E-F)** ROS-triggered K and Dex accumulative release from K@pHSST and Dex@HSST nanomicelles within 48 h (n = 3) on incubation with PBS containing 0 and 10 mM H_2O_2. **(G-J)** The internalization (G-H) and ER co-localization (I-J) of HSST and pHSST labeled with DID in M0/M1 cells. Blue, DAPI; Red, DID-labeled HSST/pHSST; Green, ER-tracker.
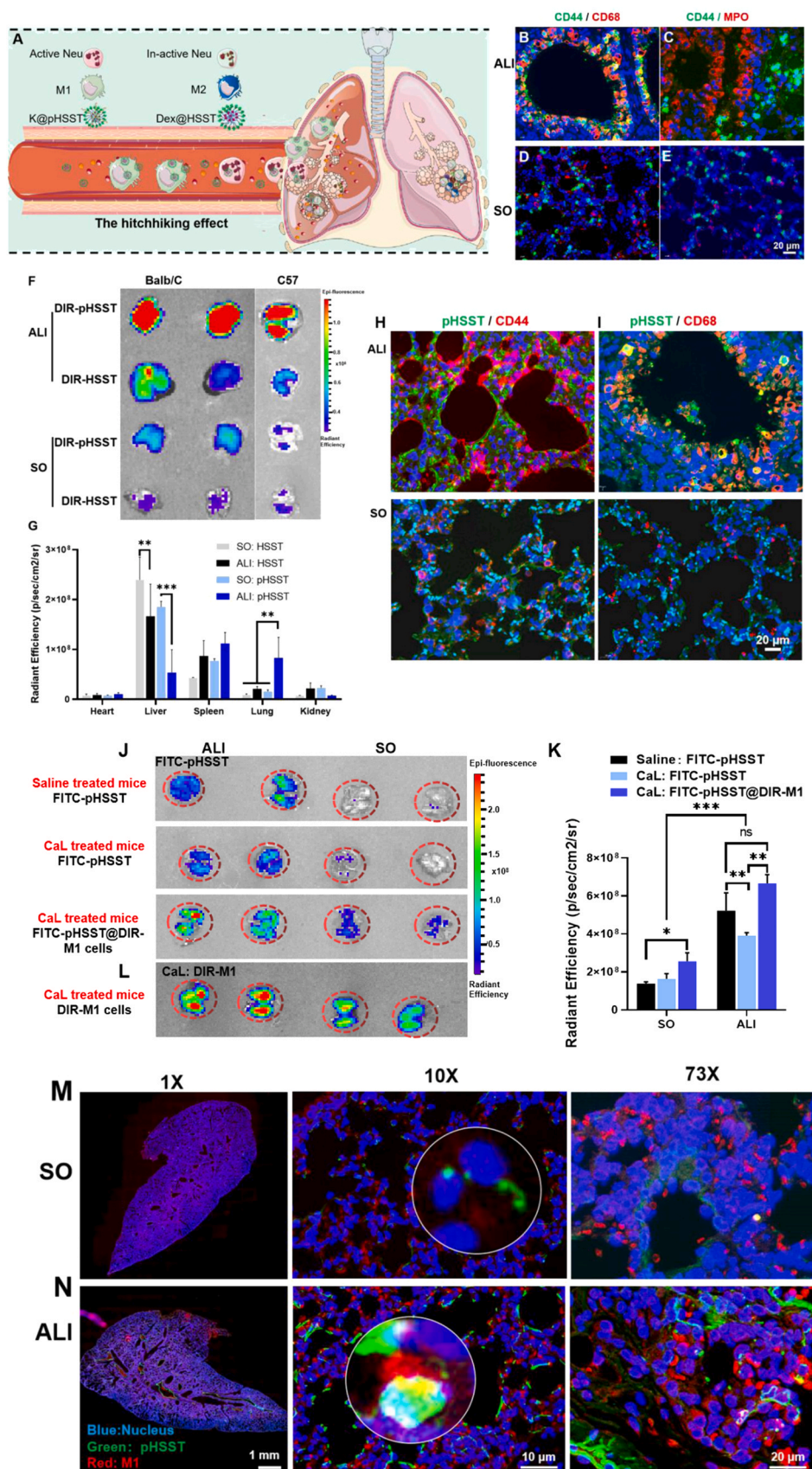
Fig. 2. pHSST selectively accumulated in the lung via hitchhiking M and Neu cells. (A) Schematic diagram of pHSST enriched into lung tissue. **(B-E)** Immunofluorescence staining of lung sections indicated the signals of CD44 (Green) and CD68 (Red) or MPO (Red). **(F-G)** Lung distribution of DIR-HSST and DIR-pHSST in ALI or SO mice. **(H-I)** Immunofluorescence staining of lung sections indicated the signals of FITC-pHSST (Green) and CD44 (Red) or CD68 (Red). **(J-L)** Lung distribution of FITC-HSST and FITC-pHSST in ALI or SO mice whose M cells were depleted. (M) Lung distribution of the adoptive M1 cells. **(M-N)** Immunofluorescence staining of lung sections indicated the location of FITC-pHSST and adoptive M1 cells in M cells depleted mice**.** Blue, nucleus; green, pHSST; Red, CD86.

(Fig. 2M-N). FITC-pHSST signal was very weak in SO mice, while an obvious signal could be observed in ALI mice, and most nanomicelles were located around the alveolus, overlapping with the signal of M cells. However, the adoptive M cells were mainly enriched in the liver and spleen in SO mice (Fig. S9 and Fig. S10). To a certain extent, it may reflect the effect of pHSST by hitchhiking M cells into inflamed lung tissue.

3. K@pHSST alleviated LPS-mediated inflammation by maintaining ERS homeostasis of M1 and Neu cells.

Activated Neu and M1 type macrophages were the main cell populations that mediate inflammation. Here, we verified that K could effectively inhibit LPS-mediated inflammation in vivo. Inactive Neu (N0) and M (M0) cells were activated by LPS stimulation to obtain N1 and M1 pro-inflammatory cells. For doses selection of KIRA 6, whose IC50 is 0.6 μM according to the manufacturer 's instruction in vitro, and the recommended dose in vivo is 2 mg/kg. Accordingly, we also drew on the doses used in our other research papers for different cells. In this manuscript, we examined the toxicity of different doses of KIRA6 at low, medium, and high doses on Neu and M cells, and finally screened 10 μg/mL for in vitro cellular assays and 2 mg/kg in vivo study (Fig. S11). The cytotoxicity experiments presented that the viability of N1 cells was inhibited by 50% after incubation with K or K-loaded nanomicelles (K@HSST and K@pHSST). The inhibition of ERS resulted in massive apoptosis of N1 cells. For M cells, it was not greatly affected by the inhibition of ERS due to their robust plasticity (Fig. 3A). Post LPS stimulation, N1, and M1 cells would accelerate the progress of inflammation by releasing a large amount of pro-inflammatory factors such as IL-1β, IL-6, and TNF-α, etc., which decreased significantly after being administrated with K, K@HSST, and K@pHSST (Fig. 3B and C). The effect of K on M1 and N1 cells was mainly achieved by inhibiting the XBP-1 protein. As shown in Fig. 3D and Fig. S12, the free K and K@pHSST could significantly down-regulate the expression of ERS-related proteins (XBP-1, CHOP, and p-PERK). Because of the reductive properties of α-TOS, pHSST alone attenuated the high ROS level of inflammatory cells (Fig. 3E), compared to that of the PBS-treated group (Control). For M1 cells, we found that ROS level was significantly inhibited by K@pHSST. The phenotype of M cells was analyzed and most of the LPS treated-M cells were polarized toward the M1 phenotype, the proportion of M1 cells was significantly reduced after being treated with free K, K@HSST, and K@pHSST, especially in the K@pHSST treated group. Although K did not sufficiently reverse the polarization of M or M1 cells towards to M2 phenotype in the inflammatory environment (Fig. 3F-H). In all, LPS-induced M1 polarization and inflammation could be alleviated by reversing the high ER stress.

4. K@pHSST alleviated inflammation of ALI mice by targeting the ERS of M1 cells.

After that, K@pHSST was used to alleviate LPS-induced ALI according to Fig. S13. LPS-elicited ALI mice had poor survival status. Within 72 h, the body weight of the saline treated-mice decreased by nearly 20% (Fig. 4A), while free K, K@HSST, and K@pHSST treated mice showed a downward trend in body weight within 48 h but began to increase afterward, which indicated that the treatment regime with K could help mice to rebuild the respiratory system and enhance the ability of daily activities. Although the average weight gain of the mice in the K@pHSST group was not optimal, the 72 h survival rate in the K@pHSST-treated group was maintained at 100%, which was only 30%– 50% in other groups (Fig. 4B). The permeability index, reflexing the damage of alveolar epithelial and endothelial permeability, was analyzed by injecting human serum albumin 1 h before mice were sacrificed. The lungs wet/dry weight ratio also returned to a relatively normal value (Fig. 4C), and the permeability

index of free K, K@HSST, and K@pHSST treated mice was prominently recovered compared with that of the saline group. Mice's alveolar leakage rate, especially in the K@pHSST group, was almost the same as that of the mice in the SO group (Fig. 4D). Micro-CT imaging was performed at 48 h after modeling, and it was found that there were multiple lung patchy shadows in saline- and free K-treated mice, and some of them had consolidation, especially in the upper lungs, while the lung tissues morphology of K@pHSST was similar to that of SO mice (Fig. 4E). After dissecting mice at the end of treatment, it was intuitive that the lungs of saline-treated ALI mice had marked congestion, while the normal physiological structure could be observed in the K@pHSST-treated mice (Fig. S14). HE staining showed that the lung tissues of the ALI mice had striking inflammatory cells infiltration, thickened alveolar septa, and normal alveolar structures were rarely observed, while the lung tissues of K@HSST and K@pHSST showed alveolar morphology (Fig. 4F). The abnormal staining of PAS sections demonstrated that the lung tissues of saline-treated mice were filled with mucus, severe tissue edema, and inflammation. Although the phenomenon was relieved after various treatments, it still did not return to normal physiology, suggesting that ALI may lead to the progression of pulmonary fibrosis (Fig. 4G). And with Masson's trichrome staining on the lung tissues, post-treatments, obvious lung injury and fibrosis were observed (Fig. S15).

5. Anti-inflammatory mechanism of K@pHSST.

In the lung tissues of saline-treated mice, a large number of M cells aggregated, most of which were M1 cells (CD68 +CD86 +). Treated with K@pHSST, the infiltration of M cells was reduced, especially the M1 phenotype cells, in turn, M2 phenotype (CD68 +CD163 +) cells increased prominently. The infiltration of Neu was an important indicator of inflammation. As the inflammation subsided, Neu was phagocytosed and cleared by M2 cells. In the lung tissues of mice in the saline-treated group, there was a very pronounced infiltration of activated Neu cells compared with the other treatment groups (Fig. 5A). Then, the cells in the lung tissue were analyzed by flow cytometry. In the lung of mice in the saline group, Neu cells (CD11b+Ly-6 g/Ly-6c+) accounted for more than 60%, while the proportion of healthy mice was less than 10%. After being treated with K@pHSST, the proportion of Neu in lung tissue dropped to 38.1%. Although other treatment groups had a relatively high proportion of Neu (Fig. 5B and Fig. S16), the proportion of MPO-positive cells was lower. It indicated that although K could reduce Neu activity or mediate Neu apoptosis by inhibiting ERS (Fig. 2A), the proportion of M1 cells was higher than M2 cells in the lung tissues of Free K and K@HSST-treated mice (Fig. 5C-D), resulting in insufficient phagocytosis of apoptotic Neu, which allowed Neu to accumulate in lung tissues and exacerbate the progression of inflammation. In addition, we analyzed the T cells in the lung tissues and found a large proportion of CD4 + and CD8 + T cells infiltration in the lung tissues of saline-treated mice, which was another important resource of the inflammation-mediated immune factor storm. Fortunately, the proportion of T cells infiltrating the lung tissues of mice was effectively decreased after the treatment of K@pHSST (Fig. S16). Since K@pHSST alleviated the inflammation of ALI mainly by inhibiting ERS, ERS-related proteins in the lungs were detected and it was found that the expressions of p-PERK and XBP-1 in the lung tissues of saline treated-mice were significantly up-regulated. In addition, compared with the saline-treated mice, mice treated with free K or K@HSST, especially K@pHSST, presented significant inhibition of ERS-related proteins (Fig. 5E). Immune factor storm was one of the main factors amplifying inflammation. Here, the reductive K@pHSST could effectively resist ROS and eliminate inflammatory/immune factor storm. Fig. 5F-I showed that in serum and bronchoalveolar lavage fluid (BALF) of mice, the levels of anti-inflammatory factors such as
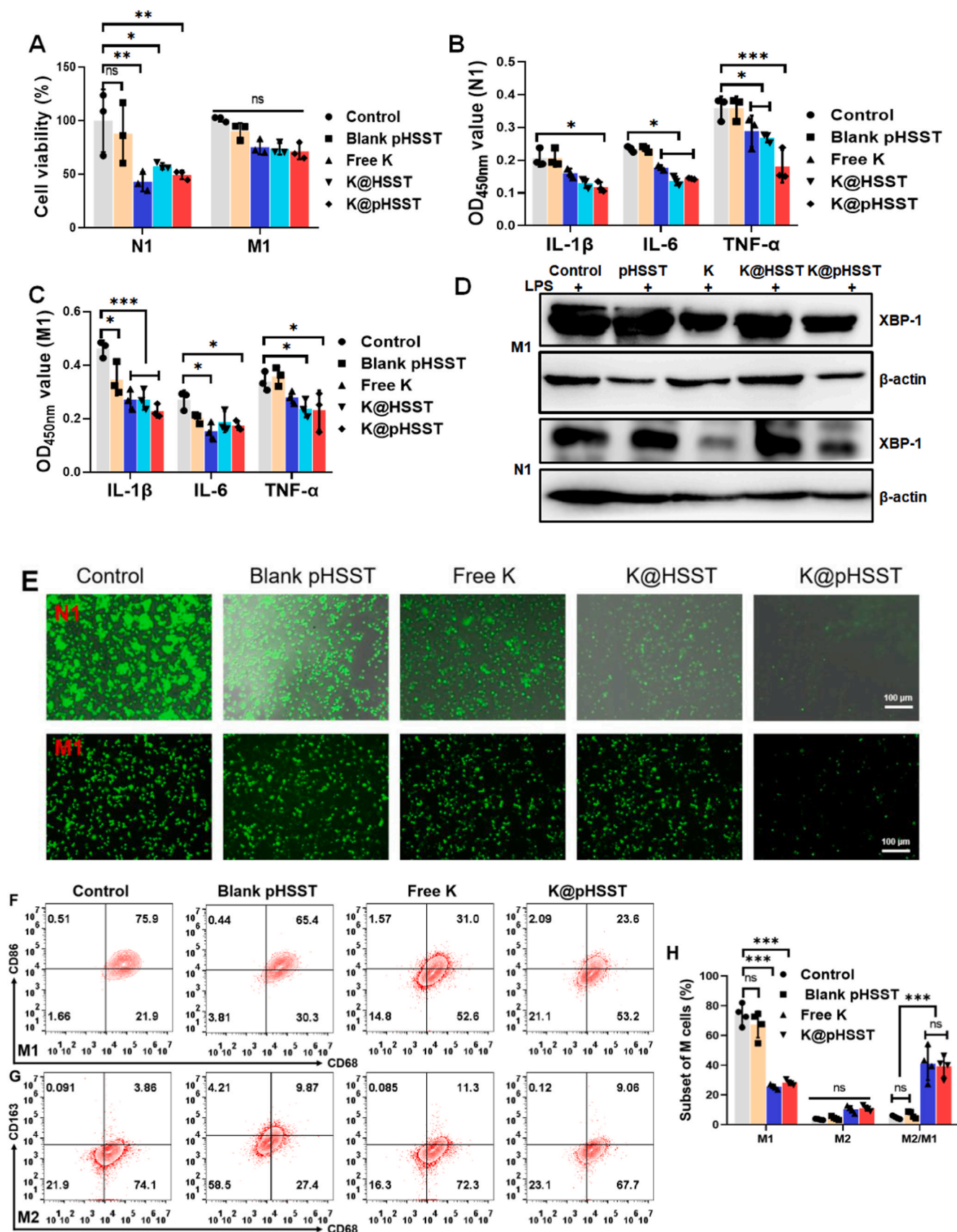
Fig. 3. K@pHSST alleviated LPS-mediated inflammation by inhibiting ERS of M and Neu cells. (A) CCK8 assay of N1 and M1 cells treated with K@pHSST and other control groups. (B-C) Elisa assay of proinflammatory factor released from K@pHSST treated N1 (B) and M1 (C) cells. (D) Western blotting assay of ERS-related proteins expressed in K@pHSST treated N1 and M1 cells. (E) Immunofluorescence test of ROS released from K@pHSST treated N1 and M1 cells. (F-H) Representative flow cytometry analysis plots (F-G) and quantification (H) of phenotypic changes of M1 cells after being treated with K@pHSST.
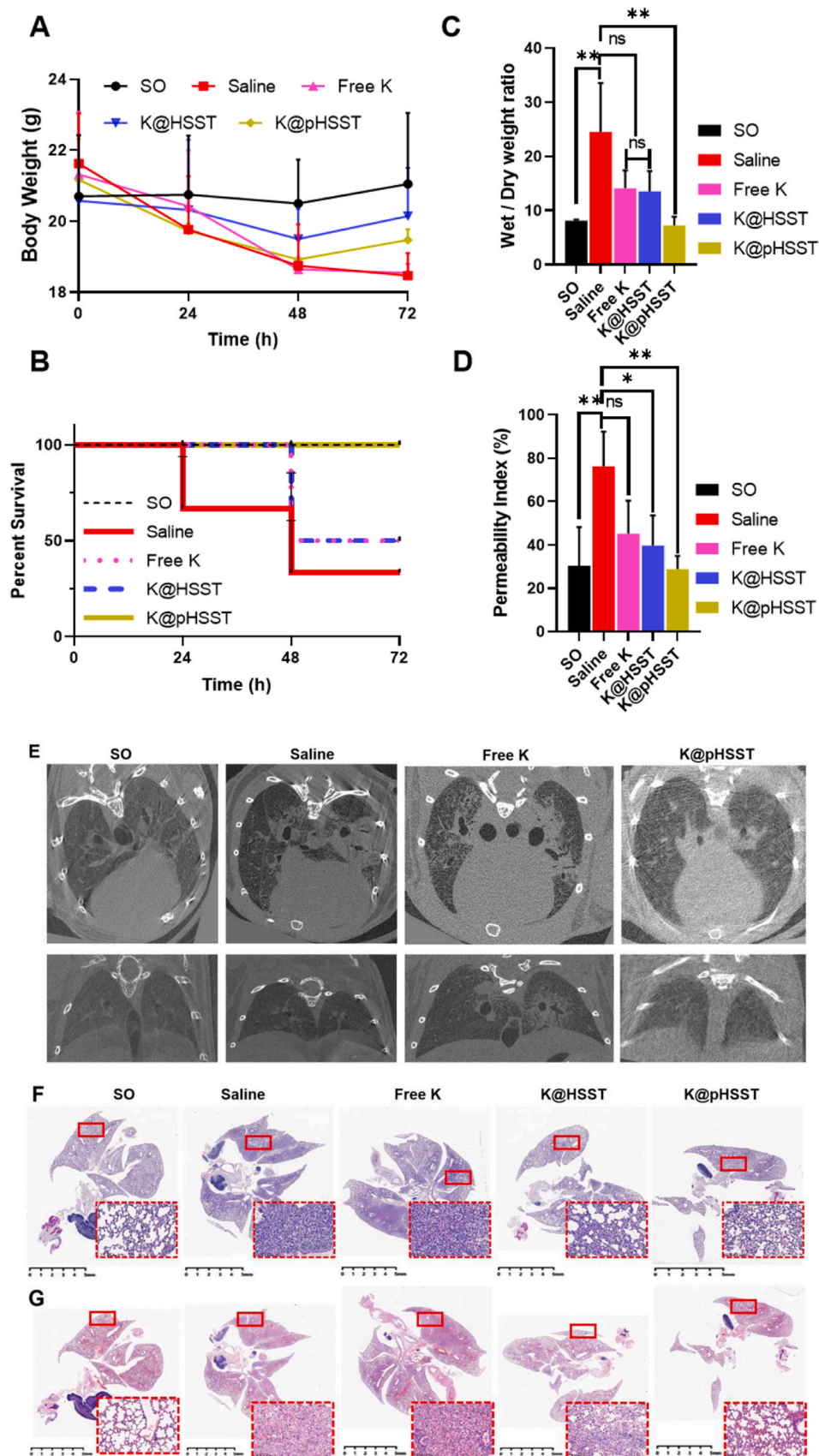
Fig. 4. K@pHSST alleviated inflammation in ALI mice by targeting the ERS of M1 cells. (A) Weight change curve during treatment. (B) Survival rate curve during treatment. (C) Permeability index after the treatment. (D) Wet/dry lung weight ratio after treatment. (E) Micro-CT of lung tissue at 48 h. (F) HE staining of lung tissue after treatment. (G) PAS staining of lung tissue after treatment.
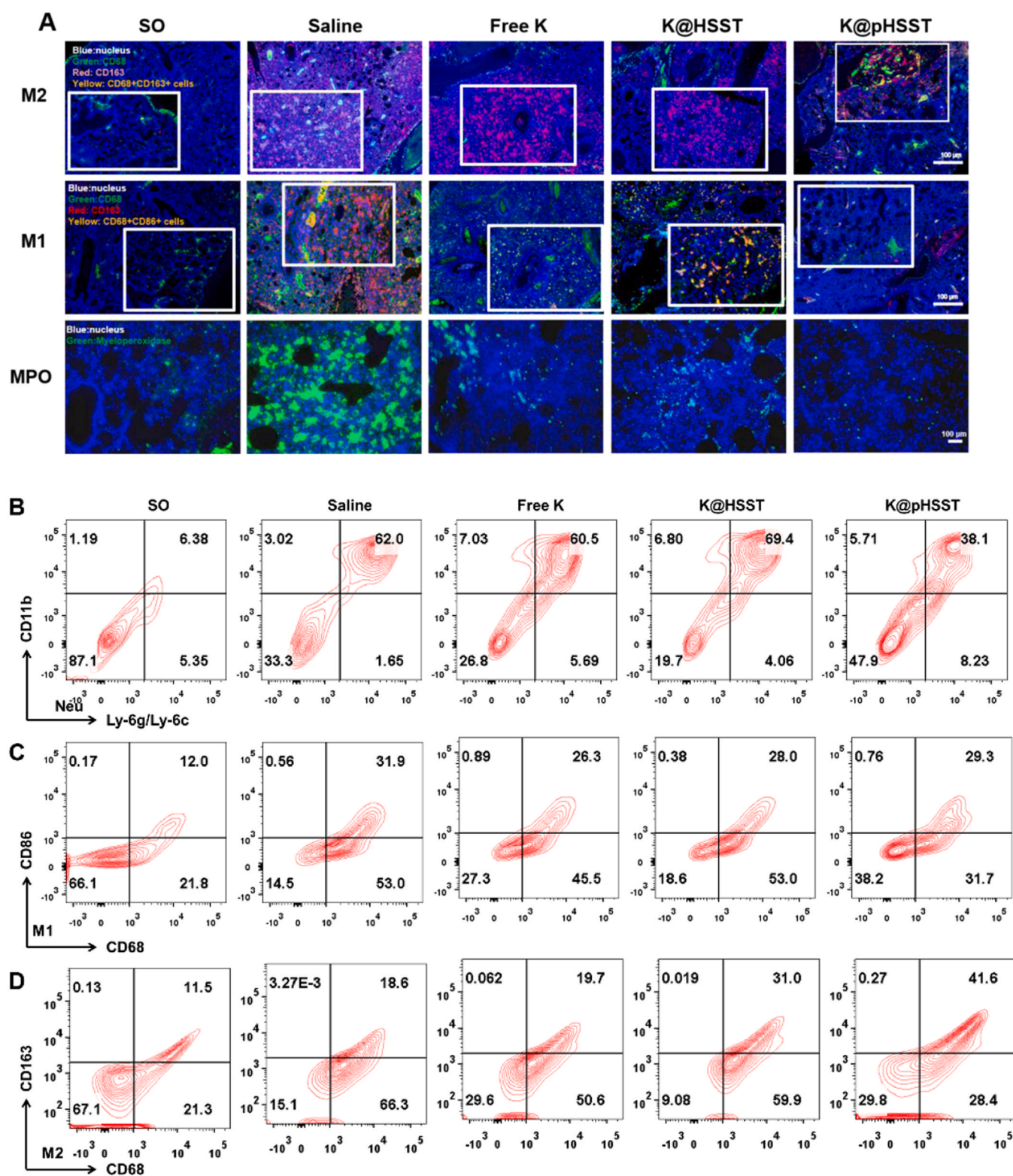
Fig. 5. Anti-inflammatory mechanism analysis of K@pHSST. (A) Immunofluorescence sections of lung tissue indicate the infiltration of M and Neu cells. (B-D) Flow cytometry analysis of Neu (B), M1 (C), and M2 (D) cells in the lung tissues. (E). Immunofluorescence sections of lung tissue indicating ERS-related proteins. Blue: nucleus; Green: pPERK or anti-XBP-1. (F-I). ELISA assays for the level of major immune factors in the serum (F-G) and BALF (H-I).

IL-4, IL-10, and TGF-β were up-regulated, which also favored the M2 polarization and promoted inflammation resolution. Inflammatory factors were mainly secreted by Neu and M1 cells. After K@pHSST treatment, the levels of related inflammatory factors such as TNF-α, IL-17A, and IL-1β were decreased.

6. K@pHSST effectively suppressed inflammation responses and fibrosis in combination with Dex@HSST

The main factor driving the development of ALI into pulmonary fibrosis is the infiltration of chronic inflammation, which lead to the
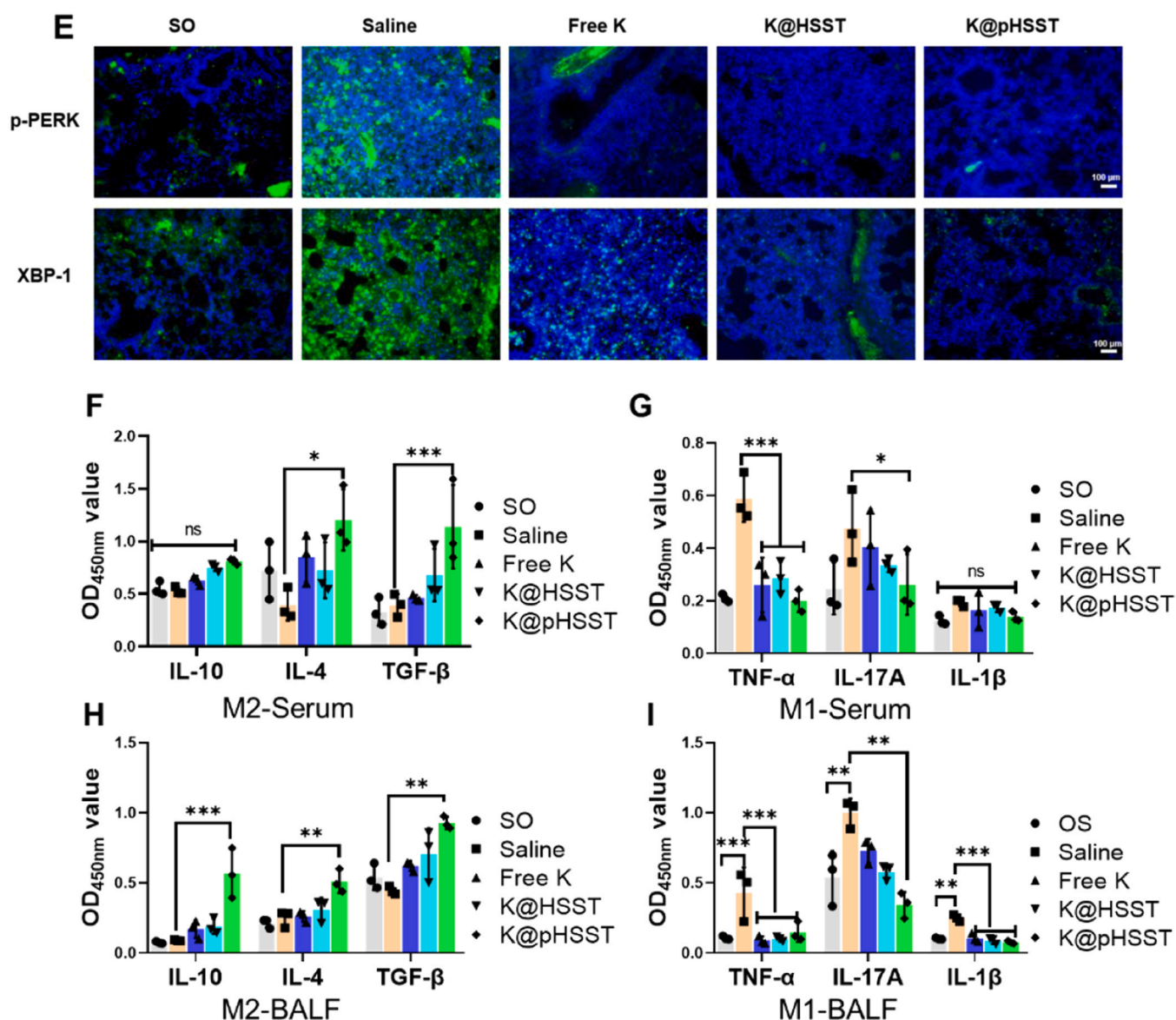
Fig. 5. (*continued*)

continuous activation of TGF-β/smad signaling that results in the hyperpolarization of M2 cells. Therefore, the main strategy for suppressing PF is to eliminate inflammation and prevent the hyperpolarization of M2 cells. At present, Dex is one of the main hormonal drugs clinically used for ALI/ARDS, which is helpful for inflammation elimination. However, the severe toxicity and side effects of Dex greatly limit its clinical application. For the selection of Dex dose, we also referred to the relevant literature and conducted simultaneous low, medium and high dose studies, and finally selected 5 μg/mL for in vitro cellular assays and 2.5 mg/kg for in vivo studies [47–49]. We chose low doses for pharmacodynamic studies based on effectiveness, and the final HE sections of each organ showed that the doses we chose did not cause significant toxic effects on important tissues (Fig. S17 and Fig. S18).

According to the above results, we prepared Dex@HSST, which could deliver Dex into cells and release drugs in response to high-level intracellular ROS. The anti-fibrosis effect of K@pHSST in combination with Dex@HSST was then investigated. Dex@HSST showed a good scavenging effect on intracellular ROS, which can be further amplified in M1 cells in combination with K@pHSST (Fig. 6A), and the release of pro-inflammatory cytokines was also inhibited

(Fig. 6B). Since Dex enhanced M2 polarization, it played an important role in promoting ALI/ARDS into an effective repair stage [50]. From the in vivo results, in the context of LPS-mediated inflammation, Dex@HSST down-regulated the proportion of M1 cells and promoted M2 polarization (Fig. 6C, D), which was a key indicator of rapid recovery from ALI.

However, excessive M2 polarization could lead to fibrosis. To further study the anti-fibrotic effect of Dex@HSST combined with K@pHSST, M2 cells were co-incubated with NIH3T3 cells, and then received various treatments (Dex@HSST, K@pHSST, and Dex@HSST plus K@pHSST, etc.) (Fig. 6E). The levels of fibrosis-related cytokines after treatment of K or Dex alone could not be reduced in the co-culture system, but Dex@HSST combined with K@pHSST could significantly inhibit the secretion of IL-4, TGF-β, and MMP-7 (Fig. 6F). The expressions of fibronectin, collagenase type-1, and α-SMA in the co-incubated system were markedly decreased in the combining-treating group (Fig. 6G). The migration of M2 cells induced by the activation of NIH 3T3 was dramatically inhibited by the combination of Dex@HSST and K@pHSST (Fig. 6H). Repolarization from M2 to M1 was also detected after being treated with Dex and K, especially in the Dex@HSST plus K@pHSST treated group (Fig. 6I-J).

7. Dex@HSST effectively suppressed bleomycin-induced PF in combination with K@pHSST

As mentioned above, K@pHSST could specifically target Neu and M1 cells to reverse their high ERS, thereby inhibiting the activity of Neu and the polarization phenotype of M1 cells for effectively alleviating the inflammation of ALI. However, Masson staining results of lung tissues in Fig. S15 revealed that mice treated with K@pHSST exhibited certain fibrotic lesions, due to the insufficient influence of K@pHSST on the polarization of M2 cells. Therefore, to prevent ALI from progressing to PF, it was necessary to increase the number of pro-reparative M2 phenotype cells in the inflamed lung. Dex, a glucocorticoid, not only has a strong anti-inflammatory effect but also acts as a stimulator of M2 polarization, which plays an important role in preventing PF occurrence. Dex@HSST and K@pHSST, then, were adopted in combination for the treatment of PF model mice induced by bleomycin (BLM) (Fig. S19). During the 4 weeks of treatment, the body weight of saline-treated mice decreased severely (Fig. 7A), with 60% of the mice losing more than 20% of their body weight, which was considered as dead, while the survival rates of mice in the other groups were at least 80%, indicating that only less than 20% of the mice were underweight (Fig. 7B). Whereas the

increased weight ratio of lung/body indicated the progression of inflammation, which showed no significant difference between Dex@HSST plus K@pHSST group and SO treated mice (Fig. 7C), suggesting a physiological recovery of lung tissues. To evaluate the anti-inflammatory effort of Dex@HSST plus K@pHSST, the levels of inflammatory factors such as IL-4, IL-10, MMP-7, and TGF-β were assayed by ELISA kits on the 28th day. The levels of relevant immune factors after combined administration were the same as those of SO mice, which indicated that the treatment of Dex@HSST plus K@pHSST was beneficial for anti-inflammatory and anti-fibrosis. Besides, IL-17A was the main pro-inflammatory factor, which was explosively secreted in the saline group compared to other groups, indicating that the bleomycin-induced PF model mice were in a long-term chronic inflammation (Fig. 7D). During the treatment, it could be seen from the micro-CT images that increased lung tissue density and fibrous connective tissue deposition in the lungs of the saline-treated mice. In contrast, the deposition of pulmonary interstitial fibrous tissues was not obvious in the Dex@HSST plus K@pHSST treated mice (Fig. 7E). Pictures in Fig. 7F also displayed that the lung volume of the mice in the saline group was increased, accompanied by obvious tissue congestion and edema. The results of Masson staining further showed that, except for the SO group and
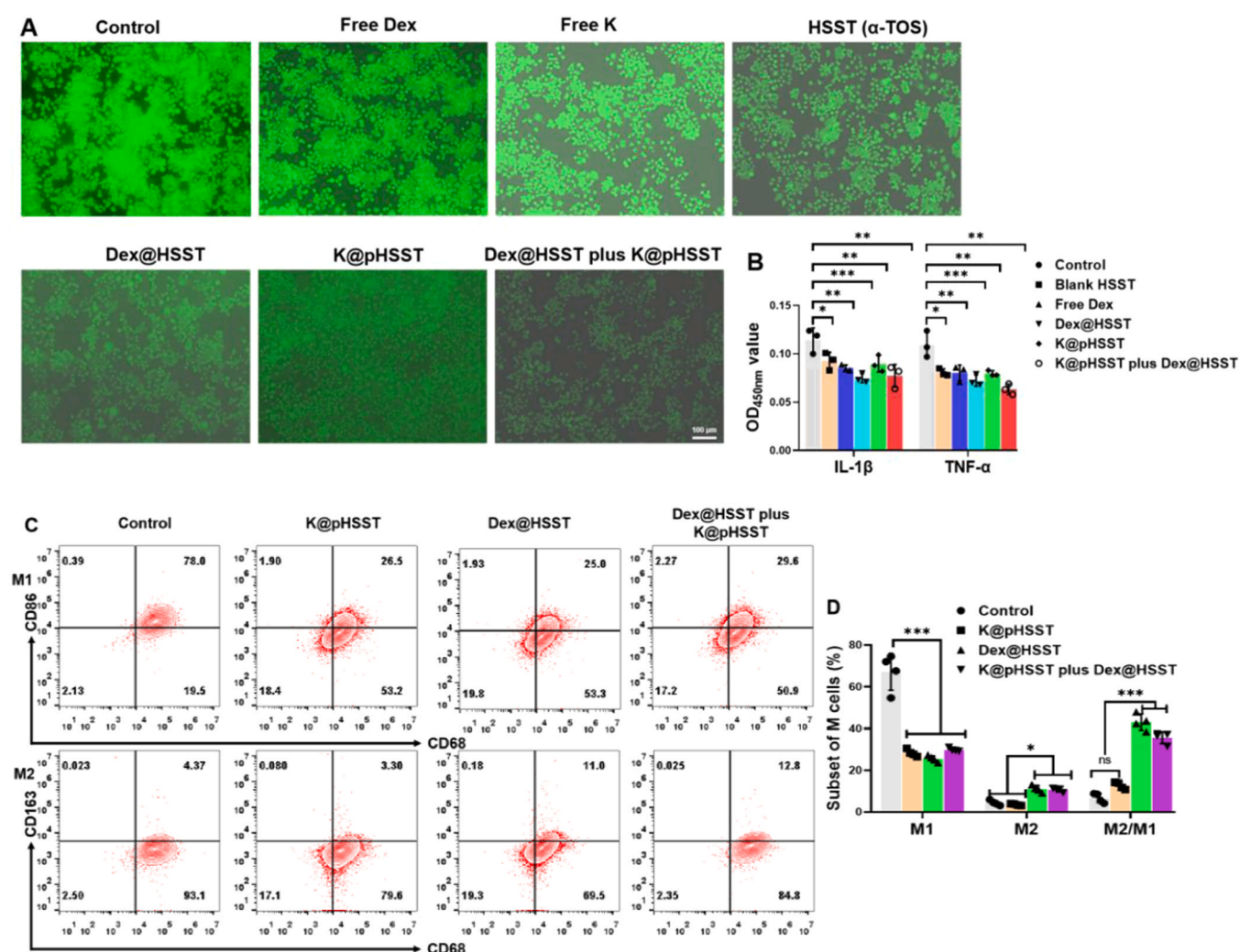
Fig. 6. K@pHSST effectively suppressed inflammation response and fibrosis in combination with Dex@HSST. (A) Immunofluorescence test of ROS released from M1 cells. **(B)** Elisa assay of proinflammatory factors released from M1 cells. **(C-D)** Flow cytometry analysis (C) and quantification (D) of phenotypic changes of M1 cells after being treated with Dex@HSST plus K@pHSST. **(E)** The schematic diagram of the M2 and NIH3T3 co-cultured transwell system. **(F)** Elisa assay of anti-inflammatory factors released from the co-cultured system. **(G)** Western blotting showed decreased levels of fibronectin, collagen I, and α-SMA proteins in the Dex@HSST plus K@pHSS treated co-cultured system. **(H)** Representative flow cytometry plots showed the M cells migrating to the lower chamber of the transwell. **(I-J)** Representative flow cytometry showed the M1 (CD68 +CD86 +) and M2 (CD68 +CD163 +) cells.
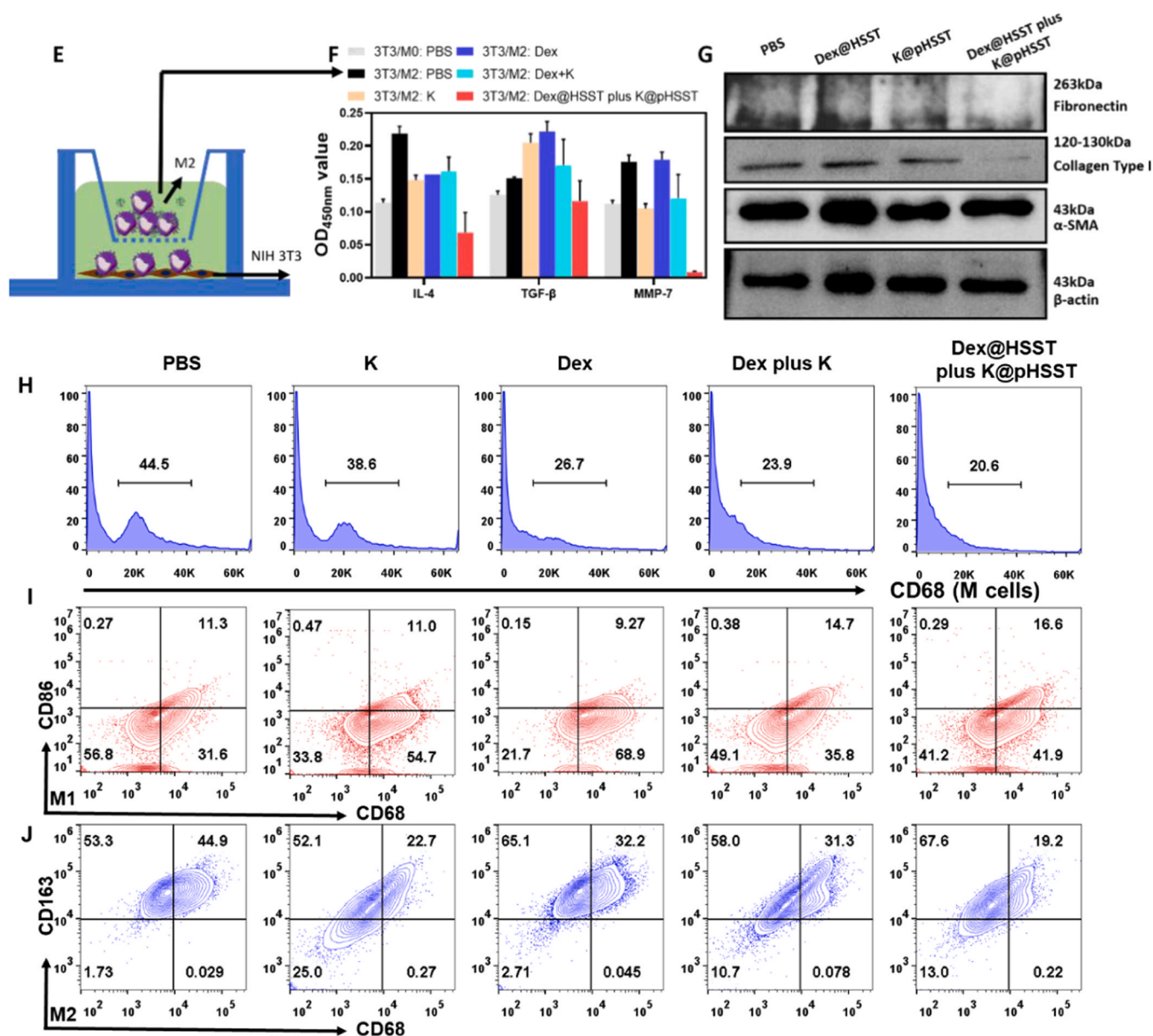
Fig. 6. (continued)

the Dex@HSST plus K@pHSST treated groups, the alveolar space became smaller and the fibrosis was severe in other groups (Fig. 7G-H). Even after receiving the free Dex, K, or a combination of these two free drugs, the lung tissues structure of the mice was still damaged, while the combined treatment of Dex@HSST plus K@pHSST effectively repaired the structure of alveoli (Fig. 7I-J).

8. Dex@HSST and K@pHSST anti-fibrosis by restoring ERS homeostasis

The expression of α-SMA is a characteristic feature of activated fibroblast cells and is generally considered as a biomarker of PF. The immunohistochemical staining results showed that compared with other groups, the expression of α-SMA, as well as the level of fibronectin, was dramatically inhibited in Dex@HSST plus K@pHSST treated group (Fig. 8A). However, the expression of fibronectin in lung slices of mice treated with Dex was up-regulated, which could

be attributed to the Dex-induced excessive repair and exacerbated fibrosis (Fig. 8B). In addition, Dex@HSST plus K@pHSST treated mice showed larger areas of collagen-1 deposition than untreated PF mice, which exhibited greater fibronectin than other mice based on immunohistochemical staining (Fig. 8C).

The imbalance of M2/M1 was the major factor in PF. From Fig. 8D-E, it could be seen that the combined treatment of Dex@HSST plus K@pHSST was beneficial to restore the ratio of M1/M2 cells in lung tissue. Neither free Dex nor K could effectively reverse the high proportion of M2 in the lung tissue of mice with bleomycin-induced PF. According to our hypothesis, the reversal of macrophage polarization imbalance was mainly achieved by restoring its ER homeostasis. Two ERS markers, XBP-1, and p-PERK, were detected here, and as expected, the XBP-1 and p-PERK pathways of UPR were dramatically activated in saline- and Dex- treated mice (Fig. 8F-G), and the excessive ERS in lung tissue was effectively alleviated by K, specific inhibition of XBP-1.
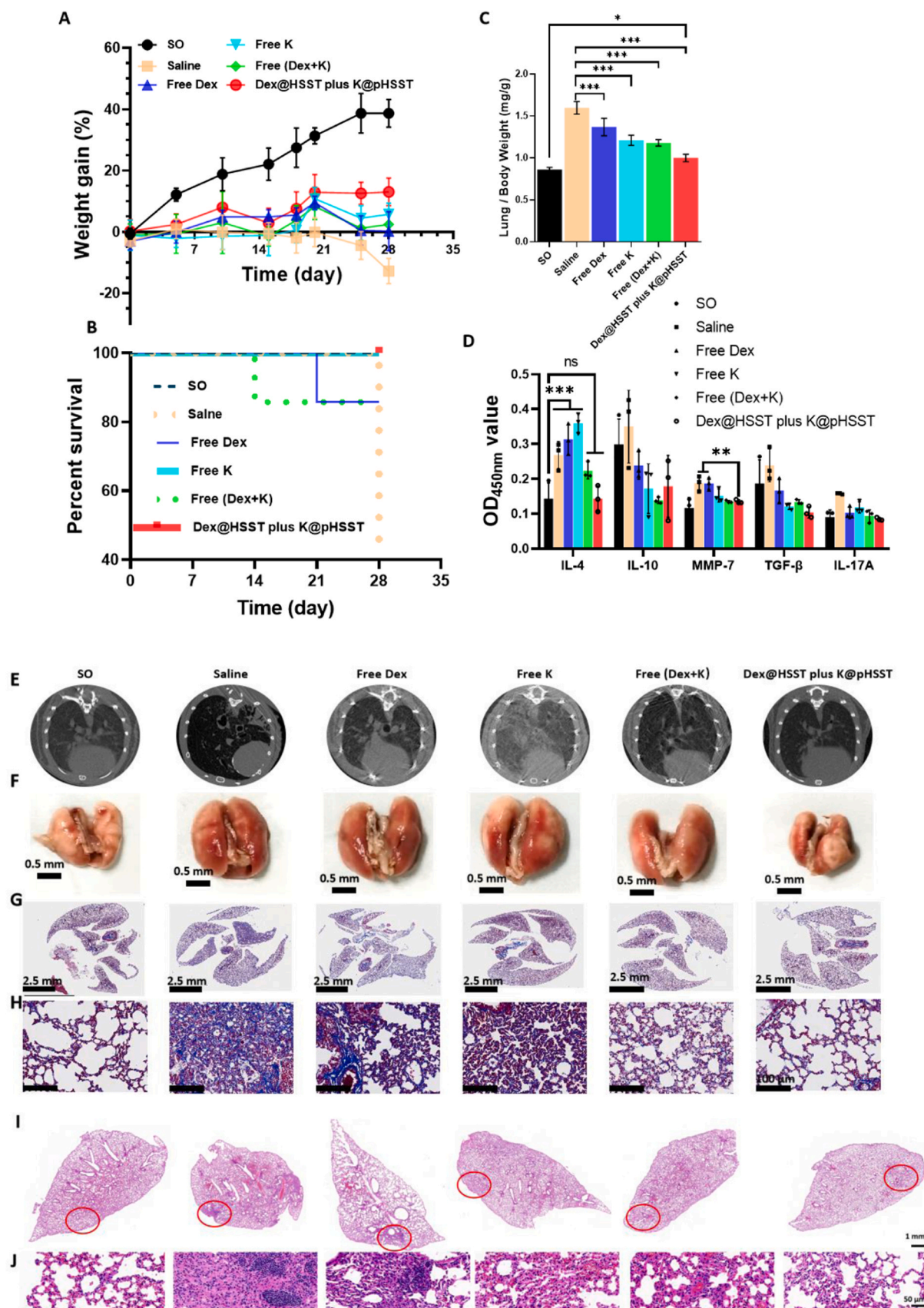
Fig. 7. K@pHSST effectively suppressed bleomycin-induced pulmonary fibrosis in combination with Dex@HSST. (A) The body weights of the mice were recorded regularly. (B) The survival rate of mice after various treatments. (C) The lung index was analyzed on the 28th day after various treatments. (D) The expression of inflammatory cytokines in mice serum. (E) Micro-CT image of lungs. (F) Representative picture of lung isolated from mice post various treatments. (G) Representative full scan images of Masson's trichrome staining of lung sections after various treatments. (H) Representative enlarged image based on G. (I) Representative full scan images of H&E staining of lung sections after various treatments (The red circle indicated the enlarged part). (J) Representative enlarged images from me.
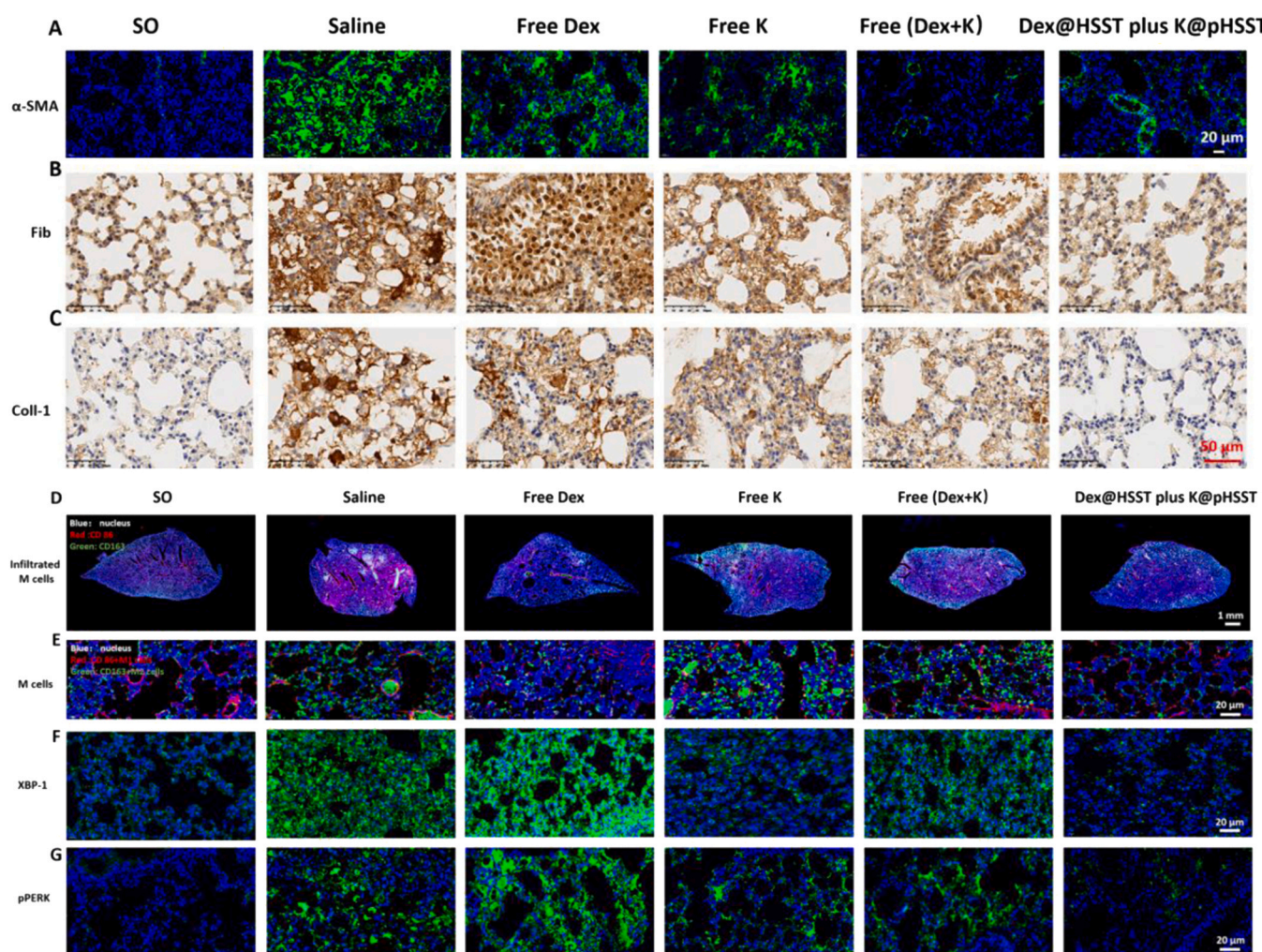
Fig. 8. Dex@HSST and K@pHSST resist fibrosis by restoring ERS homeostasis. (A-C) Representative images of immunostaining and immunohistochemistry for alpha-smooth muscle actin (α-SMA), Fibronectin (Fib), and Collagen I (Coll-I) in lung tissue sections. (D-E) Images of immunostaining for CD86 + M1 and CD163 + M2 cells. (F-G) Images of immunostaining for ER-stress-related proteins.

Conclusion and discussion

In this study, we focus on macrophages, which are recognized as the key drivers of inflammation in ALI/PF. As macrophages are involved in the etiology of ALI/PF and regulate inflammatory cascades, we propose that they are a promising therapeutic target. Here, we have synthesized step-wised targeting HA-based drug carrier, pHSST, which can rapidly and effectively accumulate in the ALI lungs, especially around the pulmonary alveoli. The ALI lung accumulation of pHSST is first attributed to the "hitchhiking" effect of the M and Neu cells and then is preferentially internalized by injured alveolar epithelial cells and alveolar macrophages through CD44-mediated endocytosis. CD44 has received much attention in studies about tumor targeting and metastases mechanisms of cancer. However, it is a new field for CD44 as a drug target in the ALI and PF.

As the main driver for ALI and PF, macrophages are accompanied by a high level of ERS, which triggers the inflammation of M1 and the over-reparation of M2. Homeostatic repair of ERS is a key to reversing M1/M2 hyperpolarization. Therefore, we use IRE1/XBP-1-specific inhibitor KIRA 6 to mitigate excessive ERS in macrophages and neutrophils. As one of the UPR pathways, IRE-1/XBP-1 is involved in the M1-mediated inflammation in various chronic diseases, such as lupus and inflammatory bowel disease[51]. In addition, the activation of IRE-1/XBP-1 inhibits cell glycolysis,

promotes oxidative phosphorylation (OXPHOS), and facilitates intracellular lipid accumulation, which in turn shapes the typical phenotype of M2 cells. Inhibiting the IRE-1/XBP-1 pathway can repolarize M2 to M1 by increasing glycolytic metabolism and suppressing fatty acid oxidation (FAO) [28,52]. Thus, IRE-1/XBP-1 is an excellent target for both ALI and PF therapy. However, since beneficial and harmful inflammation induced by ERS may coexist, or one may dominate, it is difficult to clear harmful inflammation while preserving the beneficial one. Simultaneously, there is considerable overlap between the UPR signaling pathway, which may lead to cell death and inflammatory processes. Therefore, precise targeting is necessary for the treatment of ERS-induced diseases[53,54]. And, thus, pardaxin is applied here to subtly endow the carrier with ER-targeting, on which we have done a lot of research before[39].

At present, Dex is still the first-line medication for ALI/ARDS or PF [26,55–57]. However, the latest clinical studies have shown that the therapeutic effect of Dex has the characteristics of a "double-edged sword". When combined with GRs, a low dosage of Dex can play a pro-inflammatory role by antagonizing NF-κB, enhancing the polarized number of M2 cells, and accelerating the resolution of lung inflammation and edema. Although Dex can effectively relieve excessive inflammation in the initial stage of PF and reduce the number of ventilated patients, it shows little effect on the high lethality of ALI/ARDS or PF [58]. What's more, Dex is prone to induce

M2-hyperpolarization. With the nanocarrier strategy here, it can effectively and precisely deliver Dex into inflammatory cells, and synergistically eliminate cytokine storm through the antioxidant effect of α-TOS. Combined with the reparation of ER homeostasis, it can also effectively prevent the hyperpolarization of M2, and finally, correct the lung tissue back into a normal self-repair process.

For nanomicelles to have clinical translation potential, the complexity in their design and development also needs to be minimized as much as possible to create systems that are able to be reproducibly prepared and characterize. Compared to nanoformulation co-loaded with different drugs, the preparation process of single drug-loaded nanocarrier is simpler, with better stability and easier to achieve quality control. Moreover, the physical mixing of the two nanoformulation facilitates clinical dose control and dosing regimen design, providing more flexibility in clinical applications.

The in vivo distribution data of the nanomicelles show that the in vivo fate of nanoformulation is influenced by the health and disease state of the host. In this manuscript, most of the HSST accumulated in the liver of mice, suggesting some toxicity regarding liver metabolism of this nanomicelles. While pHSST were most accumulated in the spleen and lung of the ALI mice due to the inherent immune disorders of the inflammatory microenvironment. Also, since the intervention of KIRA 6 and Dex on the immune system, such as influence the fate of DC and T cells, and the polarization of macrophages, it is suggested that we should examine the immune system toxicity when considering clinical translation.

In conclusion, based on the characteristics of ALI and PF diseases, a safe and reliable precise targeting therapeutic strategy was designed here, with which, we can effectively prevent ALI mice from progressing to PF. And the precisely step-wised targeting delivery strategy can also be applied for the treatment of other fibrotic diseases, such as renal fibrosis.

Methods

Materials

Sodium HA (molecular weight: ~5700 Da) was purchased from Freda Biochem Co., Ltd. (Shandong, China). 1-Ethyl-3 (3-dimethyl aminopropyl) carbodiimide (EDC), NHS, CYS, 1,6-diaminohexanedihydrochloride, α-TOS, were purchased from Aladdin Reagent Database Inc. (Shanghai, China). Distearoyl-sn-glycerol-3-phosphoethanolamine-N- [maleimide (polyethylene glycol)− 2000] (DSPE-PEG 2000-NH$_2$) were obtained from Shanghai AVT Co., Ltd. ER-targeting polypeptide Pardaxin[44] (PAR, sequence: H-GFFA-LIPK-IISSPLFKTLLSAVGSALSSSGGQE-OH) was synthesized by Shanghai Qiang Yao Biotech Co., Ltd. DSPE-PEG 2000-PAR was obtained by acetylation reaction between the amino group of DSPE-PEG2000-NH$_2$ and the carboxyl group of pardaxin polypeptide. IL-4, IL-6, IL-12 *et.al* ELISA kits were purchased from Jiangsu Meimian industrial Co., Ltd. Antibodies for flow cytometry analysis, such as CD68 (Cat. no.137014, Clone FA-11), CD86 (Cat. no.105007, Clone GL-1), CD163 (Cat. no.156704, Clone S15049), CD3 (Cat. no.100204, Clone 17A2) CD4 (Cat. no. 100408, Clone GK1.5) and CD8 (Cat. no. 100712, Clone 53–6.7) were purchased from Biolegend (CA, USA).

Mice and cells

Wild-type Balb/C mice (Male, 6–8-week-old) were purchased from SHANGHAI SLAC Laboratory Animal Co., Ltd. All animal studies were conducted in compliance with protocols that had been approved by the Institutional Animal Care and Use Committee of Zhejiang University. NIH3T3 cell line and RAW264.7 (mouse monocyte macrophage leukemia cells) were purchased from the Institute of Biochemistry and Cell Biology. Bone-marrow-derived macrophage (BMDMs) were isolated from femurs of mice and were cultured in

RPMI-1640 supplemented with 10% FBS, 100 U/mL penicillin-streptomycin, 50 μM β-mercaptoethanol, 20 ng/mL murine macrophage colony-stimulating factor (M-CSF1) and 1 ng/mL IL-4 or 10 ng/mL LPS (PeproTech).

Fabrication of K@pHSST and Dex@HSST

The specific experimental steps of HSST as described in the previous study[44]. Par-modified ER-targetable HSST loaded with K (K@pHSST) as well as Dex@HSST were fabricated with the solvent evaporation method. Briefly, a certain amount of DSPE-PEG-PAR and K was precisely weighed and dissolved in ethanol. Another 50 mg HSST was dissolved in 2 mL of pure water. Under magnetic agitation, a mixture of K and DSPE-PEG-PAR was added dropwise to aqueous solutions of HSST (where PAR: K: HSST=0.5:5:50, W/W) and stirred at room temperature for 24 h to evaporate the ethanol. Afterward, the aqueous solutions were probed 100 times under an ice bath (400 W, working for 2 s, intermittent for 3 s), The unloaded K and DSPE-PEG-PAR were removed by centrifugation at 4000 rpm for 10 min and further filtered through a microporous membrane with 0.45 μm pores. Similarly, Dex@HSST, DID or DIR labeled HSST and pHSST were then fabricated. The amount of K and Dex in the micelles was determined with a UV–VIS and high-performance liquid chromatography (HPLC) method respectively. The size and zeta potential of the micelles were measured using DLS using a Zetasizer (3000 HS; Malvern Instruments Ltd.). The morphology of the micelles was examined by TEM (JEOL JEM-1230 microscopes at 120 kV; JEOL, Japan).

ROS triggered the release of K and Dex from K@pHSST and Dex@HSST

The in vitro release profiles were studied by dialyzing K@pHSST and Dex@HSST (10 mg/mL) in PBS (pH 7.4) containing 1.0 M sodium salicylate (15 mL) and different H$_2$O$_2$ concentrations (0 and 10 mM) with horizontal shaking (100 rpm) at 37 °C. At predetermined time intervals, the entire medium outside of the dialysis tube was collected and replaced with a fresh buffer solution. The samples were ultra-centrifugated, and the drug concentration was determined using a UV–VIS or HPLC.

Cell internalization and ER localization

M and Neu were cultured with 100 ng/mL LPS for 24 h to obtain M1 macrophages and N1 neutrophil cells, which were then incubated with DiD-labeled HSST, DiD-labeled ER-targetable pHSST for 24 h. The cell nuclei were stained with DAPI for 15 min and fixed with 4% paraformaldehyde, followed by the observation using confocal microscopy (AIR, Nikon, Japan). To investigate the subcellular localization of the particles, cells were first incubated with DiD-HSST and DiD-pHSST for 24 h, followed by staining of ER with ER-green tracker (Beyotime, Shanghai), respectively. Co-localization of nanomicelles and organelles was determined using confocal microscopy.

In vivo biodistribution and lung targeting

SO and ALI mice were randomly divided into 2 groups respectively, which were administrated with DIR-HSST and DIR-pHSST via the tail vein (200 μg DIR/kg mouse body weight). At 6 h, mice were photographed with an in vivo imaging system (IVIS Spectrum, Caliper Life Sciences, USA). Afterward, they were anesthetized and perfused with saline, and then the major organs were excised and imaged again using the in vivo imaging system (IVIS). *Ex vivo* fluorescent images were analyzed semi-quantitatively to determine the average fluorescence intensity of the lung. To study the mechanism of lung targeting effect of pHSST. Lung tissue was sectioned and immunofluorescence staining was performed with anti-CD44

antibodies, anti-CD68 antibodies, and MPO. To further investigate pHSST targeting inflammatory lungs via M hitchhiking method. Clodronate liposomes were used to deplete macrophages in vivo, and DIR-labeled M1 cells were incubated with FTIC-HSST or FITC-pHSST for 24 h and then were imaged with the IVIS. Immunofluorescence sections were further used to study the distribution mechanism of the nanomicells in vivo.

K@pHSST and Dex@HSST alleviated inflammation by maintaining ERS homeostasis of M1 and N1 in vitro

BMDMs were isolated and cultured as previously described[28]. Briefly, bone marrow cells were isolated from the femurs and tibias of Balb/C mice. Cells were maintained in RPMI 1640 medium for 7 days and allowed to differentiate into mature macrophages[59]. Polarization of BMDMs was induced for M1 activation by treatment with LPS (100 ng/mL, Sigma) or M2 activation with IL-4 (20 ng/mL, Peprotech) for 24 h or the desired periods before further biochemical analysis. For isolation of murine Neus, bone marrow was flushed from the bone with phosphate-buffered saline (PBS), centrifuged at 1300 rpm for 4 min, and resuspended in 1 mL PBS. Density gradient centrifugal fluid was prepared by carefully pouring 2 mL 75%, 65%, 55% (v/v) Percoll (Pharmacia) mixture solution successively, and 1 mL unicellular suspension at the top. The Neus were gathered at the interface of the 65% and 75% fractions by centrifugation at 2000 rpm for 25 min, and then, the cells were washed with ice-cold PBS thrice to wash off residual Percoll solution. The Neus were cultured in a culture dish at 37 °C in a humidified atmosphere containing 5% CO_2 with RPMI 1640 medium containing 1% penicillin/streptomycin. Activated Neus (N1) was induced by LPS (100 ng/mL, Sigma) for 24 h. M1 and N1 cells were then seeded in a 3.5 cm dish and incubated overnight, and then treated with blank pHSST, free K, K@HSST, or K@pHSST (containing K 1 μg/mL) for 24 h. The cell viability was detected with the CCK8 kit. Fluorescent probe DCFH-DA was utilized to label ROS in the M1 and N1 cells according to the manufacturer's instructions. For Dex@HSST promoted M2 to M1 polarization, M2 and NIH 3T3 cells were seeded in a transwell plate and incubated with 5 ng/mL TGF-β1 overnight, and then treated with free Dex, free K, free K&Dex, and Dex@HSST & K@pHSST (containing Dex 5 μg/mL and K 1 μg/mL). Flow cytometry was used to detect the M2 cells migrated to the lower chamber.

Western blotting

BMDMs, Neu, and RAW264.7 cells were lysed according to the lysis protocol in an ice-cold radioimmunoprecipitation assay. The concentration of protein was tested using a BCA protein assay kit. Equal amounts of proteins for each group were loaded on SDS–polyacrylamide gel electrophoresis gels. Following electrophoresis, the membranes were then probed overnight at 4 °C with primary antibodies for XBP-1, p-PERK, Chop, Asma, Coll-1, and Fib (1:1000). After being washed, the membrane was incubated with appropriate secondary antibody (the secondary ant-rabbit IgG HRP; 1:1000) for 3 h at room temperature. The secondary antibody was imaged using the chemical illuminant (BeyoECL Plus) and quantified in a Bio-Rad system (ChemiDoc Touch Imaging System).

Induction of ALI model

For LPS lung injury, 100 μg LPS from Escherichia coli (serotype O111:B4; Sigma-Aldrich) in 40 μL PBS was given intratracheally. Sham-operated (SO) animals underwent the same procedure with intratracheal injection of PBS. And 4 h later after mice were grouped into six groups (N = 10): SO, saline, free K (40 μg per mice), K@HSST, and K@pHSST (containing 40 μg K for each mouse). The detailed administration information was shown in Fig. 4A. Mice were

intravenously injected at 4 h, 24 h, and 48 h after ALI model establishment. At 48 h, mice were imaged with micro CT (MILabs U-CT).

The permeability index, reflexing the damage of alveolar epithelial and endothelial permeability was evaluated by administrating human serum albumin (i.v. 25 μg; Signa-Aldrich, MO) 1 h before sacrificing the mice. The blood and analysis of bronchoalveolar lavage fluid (BALF) were collected at the time of sacrifice. ELISA assay was performed to measure the level of human albumin concentration using a human serum albumin ELISA kit (MEIMIAN, Jiangsu). The pulmonary permeability index was defined as the human albumin concentration in BAL fluid/serum ratio. The other mouse ELISA kits were used to measure the levels of TGF-β, TNF-α, IL-1β, IL-17A, and IL-4 in BALF, serum, and co-cultures according to the manufacturer's instructions.

Induction of pulmonary fibrosis

Balb/C mice were used for the induction of PF by Bleomycin (BLM, Sigma-Aldrich, USA). All operations were carried out in a clean environment. Overall, the mice were anesthetized by Intraperitoneally injection of chloral hydrate (350 mg/kg body weight). After that, the mice were operated on to expose the windpipe by blunt dissection and BLM (5 mg/kg body weight)) was dissolved in saline in advance and 200 μL of which was intratracheally administered with a 1 mL syringe injection between the tracheal cartilages, meanwhile keeping the mice upright and rotating slowly to make homogeneous drug distribution in the lung. The negative control group (SO group) was intratracheally administered 200 μL saline. This operation was repeated daily for the first three days to obtain a more reliable model of lung injury. On the 7th day, the mice randomly selected were divided into five groups (n = 4–9) and were administrated with saline, free Dex (50 μg per mice, 150 μg in total), free Dex & K, and Dex@HSST & K@pHSST (containing 50 μg dex and 40 μg K). Mice were monitored during the treatment period through micro-CT. On the 28th day, mice were imaged with micro CT (MILabs U-CT) before being sacrificed and the lungs were made to a pathological section for evaluation of the pulmonary fibrosis model.

Flow cytometry

Indicated macrophages generated in vitro were harvested and suspended in fresh PBS (10^6 cells /100 μL PBS), and incubated with fluorochrome-conjugated antibodies including FITC-anti-CD68, APC-anti-CD86, and PE-anti-CD163 for 25 min away from the light at 37 °C according to the manufacturer's instructions. And the flow cytometric detection for the abundance of M1 (CD68 +CD86 +) and M2 (CD68 +CD163 +) in lungs was operated similarly after the tissues were under grind and centrifugation. Moreover, the CD8 +T cells and CD4 +cells in the lungs were marked by FITC-anti-CD3, APC-anti-CD8, and PE-anti-CD4 after the tissues pre-treated. Subsequently, cells were washed three times to remove unconjugated antibodies and resuspended in fresh PBS for subsequent flow cytometric detection (BD Fortessa). Data were further analyzed with FlowJo V10 software.

Immunohistochemistry analysis

The lungs from mice (n = 8/group) were harvested and rinsed with PBS and then immersed into 10% buffered formalin overnight. After processing for paraffin embedding, 4 μm thick sections were prepared for hematoxylin and eosin (H&E) staining and Masson's trichrome staining using staining kits according to the manufacturer's instruction. Periodic-acid-Schiff (PAS) staining was also conducted here to diagnose the alveolar proteinosis. For analysis of relevant fibrosis indicators, paraffin-embedded lung sections were

first heated to 60 °C for 1 h, deparaffinized with xylene (3 × 5 min), and washed in different concentrations of alcohol. After retrieval of antigen and washing, the slides were blocked with peroxidase blocking buffer (DAKO Company) to block endogenous peroxidase activity. After washing the buffer (DAKO Company), Sections were incubated for 45 min at 37 °C with primary antibodies against the following antigens: anti-Coll I antibody and anti-Fib-1 antibody. The primary antibody was replaced by a buffer in negative controls. After the addition of 100 µL horseradish peroxidase-conjugated ChemMate Envision reagent, a color reaction was performed using 3,3-diaminobenzidine. Thus each section was counter-stained with hematoxylin. Tissues were measured for positive (yellowish-brown) staining and photographed under a light microscope.

Immunofluorescence staining

Mice were subjected to LPS or BLM administration and then were given therapies. At 6 h and after treatment, mice were euthanized and lungs were harvested. Lung sections were stained with DAPI and fluorescent α-SMA , CD44, CD68, CD86, and CD163 for 1 h. The staining was examined using fluorescence microscopes. For labeling ERS-related proteins, the slides were exposed to the primary antibodies [anti–XBP-1 and anti–p-PERK] and then to fluorescein isothiocyanate (FITC)–labeled secondary antibodies. Lung sections were also treated with DAPI. The staining was examined using fluorescence microscopes.

Statistical analysis

All data were presented as mean ± s.e.m. Statistical analysis was performed with unpaired two-tailed Student's t-test, or one-way or two-way analysis of variance (ANOVA) followed by Bonferroni's post-test, in GraphPad Prism 8.0. $P < 0.05$ was considered to be statistically significant.

Data availability

Data will be made available on request.

Declaration of Competing Interest

The authors declare that they have no known competing financial interests or personal relationships that could have appeared to influence the work reported in this paper.

Acknowledgments

Appendix A. Supporting information

Supplementary data associated with this article can be found in the online version at doi:10.1016/j.nantod.2022.101719.

References

[1] M.A. Matthay, R.L. Zemans, G.A. Zimmerman, Y.M. Arabi, J.R. Beitler, A. Mercat, M. Herridge, A.G. Randolph, C.S. Calfee, Nat. Rev. Dis. Prim. 5 (2019) 18.

[2] L.A. Huppert, M.A. Matthay, L.B. Ware, Semin. Respir. Crit. care Med. 40 (2019) 31–39.

[3] E. Fan, D. Brodie, A.S. Slutsky, Jama 319 (2018) 698–710.

[4] L. Zhang, Y. Wang, G. Wu, W. Xiong, W. Gu, C.-Y. Wang, Respir. Res. 19 (2018) 170.

[5] P. Cheng, S. Li, H. Chen, Cells 10 (2021) 436.

[6] Y. Guo, Y. Liu, S. Zhao, W. Xu, Y. Li, P. Zhao, D. Wang, H. Cheng, Y. Ke, X. Zhang, Nat. Commun. 12 (2021) 7094-7094.

[7] N. G. Frangogiannis. 217 (2020).

[8] X. Chen, J. Tang, W. Shuai, J. Meng, J. Feng, Z. Han, Inflamm. Res 69 (2020) 883–895.

[9] N. Barabutis, Front Med (Lausanne) 7 (2020) 344 344-344.

[10] R. Hu, Z.-F. Chen, J. Yan, Q.-F. Li, Y. Huang, H. Xu, X.-P. Zhang, H. Jiang, J. Immunol. 195 (2015) 4802–4809.

[11] W.E. Lawson, D.-S. Cheng, A.L. Degryse, H. Tanjore, V.V. Polosukhin, X.C. Xu, D.C. Newcomb, B.R. Jones, J. Roldan, K.B. Lane, E.E. Morrisey, M.F. Beers, F.E. Yull, T.S. Blackwell, Proc. Natl. Acad. Sci. 108 (2011) 10562–10567.

[12] H.J. Kim, J.S. Jeong, S.R. Kim, S.Y. Park, H.J. Chae, Y.C. Lee, Sci. Rep. 3 (2013) 1142-1142.

[13] B. Shan, X. Wang, Y. Wu, C. Xu, Z. Xia, J. Dai, M. Shao, F. Zhao, S. He, L. Yang, M. Zhang, F. Nan, J. Li, J. Liu, J. Liu, W. Jia, Y. Qiu, B. Song, J.-D.J. Han, L. Rui, S.-Z. Duan, Y. Liu, Nat. Immunol. 18 (2017) 519–529.

[14] H. Ying, K. Kang, H. Zhang, D. Zhao, J. Xia, Z. Lu, H. Wang, F. Xu, L.J.T.Jo.I. Shi, J. Immunol. (Baltim., Md.: 1950) 194 (2015) 1239–1251.

[15] N. Kapoor, J. Niu, Y. Saad, S. Kumar, T. Sirakova, E. Becerra, X. Li, P.E. Kolattukudy, J. Immunol. 194 (2015) 6011–6023.

[16] A. Croasdell, P.F. Duffney, N. Kim, S.H. Lacy, P.J. Sime, R.P. Phipps, PPAR Res 2015 (2015) 549691549691-549691.

[17] K.P. Steinberg, L.D. Hudson, R.B. Goodman, C.L. Hough, P.N. Lanken, R. Hyzy, B.T. Thompson, M. Ancukiewicz, N. Engl. J. Med. 354 (2006) 1671–1684.

[18] A. Pemmari, E.L. Paukkeri, M. Hämäläinen, T. Leppänen, R. Korhonen, E. Moilanen, Basic Clin. Pharmacol. Toxicol. 124 (2019) 404–415.

[19] P. Horby, W.S. Lim, J.R. Emberson, M. Mafham, J.L. Bell, L. Linsell, N. Staplin, C. Brightling, A. Ustianowski, E. Elmahi, B. Prudon, C. Green, T. Felton, D. Chadwick, K. Rege, C. Fegan, L.C. Chappell, S.N. Faust, T. Jaki, K. Jeffery, A. Montgomery, K. Rowan, E. Juszczak, J.K. Baillie, R. Haynes, M.J. Landray, N. Engl. J. Med. 384 (2021) 693–704.

[20] Y. Zhao, Y. Jiang, L. Chen, X. Zheng, J. Zhu, X. Song, J. Shi, Y. Li, W. He. 2020, 12 (2020) 284–295.

[21] Y. Zhang, T. Huang, L. Jiang, J. Gao, D. Yu, Y. Ge, S. Lin, Int. Immunopharmacol. 75 (2019) 105741.

[22] Y.-J. Lim, M.-H. Yi, J.-A. Choi, J. Lee, J.-Y. Han, S.-H. Jo, S.-M. Oh, H.J. Cho, D.W. Kim, M.-W. Kang, C.-H. Song, Sci. Rep. 6 (2016) 37211-37211.

[23] G. Sule, B.H. Abuaita, P.A. Steffes, A.T. Fernandes, S.K. Estes, C. Dobry, D. Pandian, J.E. Gudjonsson, J.M. Kahlenberg, M.X. O'Riordan, J.S. Knight, J. Clin. Investig. 131 (2021) e137866.

[24] C. Li, Y. Liu, Y. Li, R. Tai, Z. Sun, Q. Wu, Y. Liu, C. Sun, Int J. Mol. Sci. 22 (2021) 9997.

[25] A. Batista, J.J. Rodvold, S. Xian, S.C. Searles, A. Lew, T. Iwawaki, G. Almanza, T.C. Waller, J. Lin, K. Jepsen, H. Carter, M. Zanetti, PLoS Biol. 18 (2020) 3000687 e3000687-e3000687.

[26] K. Kamiyama, N. Matsuda, S. Yamamoto, K. Takano, Y. Takano, H. Yamazaki, S. Kageyama, H. Yokoo, T. Nagata, N. Hatakeyama, Am J Physiol Lung Cell Mol Physiol . 295 (2008) L998–L1006.

[27] J. Villar, C. Ferrando, D. Martínez, A. Ambrós, T. Muñoz, J.A. Soler, G. Aguilar, F. Alba, E. González-Higueras, L.A. Conesa, C. Martín-Rodríguez, F.J. Díaz-Domínguez, P. Serna-Grande, R. Rivas, J. Ferreres, J. Belda, L. Capilla, A. Tallet, J.M. Añón, R.L. Fernández, J.M. González-Martín, Lancet Respir. Med. 8 (2020) 267–276.

[28] M. Jiang, X. Li, J. Zhang, Y. Lu, Y. Shi, C. Zhu, Y. Liu, B. Qin, Z. Luo, Y. Du, L. Luo, L. Peng, J. You, ACS nano 15 (2021) 14522–14534.

[29] L. Liu, H.L. Johnson, S. Cousens, J. Perin, S. Scott, J.E. Lawn, I. Rudan, H. Campbell, R. Cibulskis, M. Li, C. Mathers, R.E. Black, Lancet (Lond., Engl.) 379 (2012) 2151–2161.

[30] S. Bian, H. Cai, Y. Cui, W. Liu, C. Xiao, Int J. Nanomed. 16 (2021) 2247–2269.

[31] R.T. Sadikot, A.V. Kolanjiyil, C. Kleinstreuer, I. Rubinstein, Biomed. Hub. 2 (2017) 1–12.

[32] J. Kim, G. Sahay, Nat. Nanotechnol. 17 (2022) 1–2.

[33] A.M. Sofias, Y.C. Toner, A.E. Meerwaldt, M.M.T. van Leent, G. Soultanidis, M. Elschot, H. Gonai, K. Grendstad, Å. Flobak, U. Neckmann, C. Wolowczyk, E.L. Fisher, T. Reiner, Cd.L. Davies, G. Bjørkøy, A.J.P. Teunissen, J. Ochando, C. Pérez-Medina, W.J.M. Mulder, S. Hak, ACS nano 14 (2020) 7832–7846.

[34] A.C. Anselmo, S. Mitragotri, J. Control. Release: Off. J. Control. Release Soc. 190 (2014) 531–541.

[35] N. Doshi, A.J. Swiston, J.B. Gilbert, M.L. Alcaraz, R.E. Cohen, M.F. Rubner, S.J.A.M. Mitragotri, Adv. Mater. (Deerfield Beach, Fla.) 23 (2011) H105–H109.

[36] P. Teder, R.W. Vandivier, D. Jiang, J. Liang, L. Cohn, E. Puré, P.M. Henson, P.W. Noble, Sci. (N. Y., N. Y.) 296 (2002) 155–158.

[37] S. Katoh, N. Matsumoto, K. Kawakita, A. Tominaga, P.W. Kincade, S. Matsukura, J. Clin. Investig. 111 (2003) 1563–1570.

[38] R. Farajzadeh, N. Zarghami, H. Serati-Nouri, Z. Momeni-Javid, T. Farajzadeh, S. Jalilzadeh-Tabrizi, S. Sadeghi-Soureh, N. Naseri, Y. Pilehvar-Soltanahmadi, Nanomed., Biotechnol. 46 (2018) 2013–2021.

[39] X. Yuan, B. Qin, H. Yin, Y. Shi, M. Jiang, L. Luo, Z. Luo, J. Zhang, X. Li, C. Zhu, Y. Du, J. You, ACS Central Sci. 6 (2020) 174–188.

[40] W. Li, J. Yang, L. Luo, M. Jiang, B. Qin, H. Yin, C. Zhu, X. Yuan, J. Zhang, Z.J.Nc Luo, 10 (2019) 1–16.

[41] Y. Shi, Y. Lu, C. Zhu, Z. Luo, X. Li, Y. Liu, M. Jiang, X. Liu, L. Luo, Y. Du, J. You, Biomaterials 272 (2021) 120757.

[42] Y. Shi, C. Zhu, Y. Liu, Y. Lu, X. Li, B. Qin, Z. Luo, L. Luo, M. Jiang, J. Zhang, G. Guan, C. Zhang, J. You, Adv. Healthc. Mater. 10 (2021) e2001934.

[43] H. Zhang, W. Li, X. Guo, F. Kong, Z. Wang, C. Zhu, L. Luo, Q. Li, J. Yang, Y. Du, J. You, ACS Appl. Mater. Interfaces 9 (2017) 20385–20398.

[44] C. Zhu, H. Zhang, W. Li, L. Luo, X. Guo, Z. Wang, F. Kong, Q. Li, J. Yang, Y. Du, J. You, Biomaterials 161 (2018) 144–153.

[45] H. Yin, X. Yuan, L. Luo, Y. Lu, B. Qin, J. Zhang, Y. Shi, C. Zhu, J. Yang, X. Li, M. Jiang, Z. Luo, X. Shan, D. Chen, J. You, Adv. Sci. 7 (2020) 1903381.
[46] P. Johnson, B. Ruffell, Inflamm. Allergy Drug Targets 8 (2009) 208–220.
[47] É. Azoulay, E. Canet, E. Raffoux, E. Lengliné, V. Lemiale, F. Vincent, A. de Labarthe, A. Seguin, N. Boissel, H. Dombret, B. Schlemmer, Eur. Respir. J. 39 (2012) 648–653.
[48] W. Hong, J. Yang, Z. Bi, C. He, H. Lei, W. Yu, Y. Yang, C. Fan, S. Lu, X. Peng, X. Wei, Signal Transduct. Target Ther. 6 (2021) 1.
[49] F. Terzi, B. Demirci, İ. Çınar, M. Alhilal, H.S. Erol, Respir. Res 23 (2022) 249.
[50] P.M.-K. Tang, D.J. Nikolic-Paterson, H.-Y. Lan, Nat. Rev. Nephrol. 15 (2019) 144–158.
[51] A. Kaser, A.-H. Lee, A. Franke, J.N. Glickman, S. Zeissig, H. Tilg, E.E.S. Nieuwenhuis, D.E. Higgins, S. Schreiber, L.H. Glimcher, R.S. Blumberg, Cell 134 (2008) 743–756.

[52] Y. Lu, Y. Shi, Z. Luo, X. Guo, M. Jiang, X. Li, J. Zhang, C. Zhu, H. Yin, B. Qin, X. Liu, J. Huang, Y. Du, L. Luo, J. You, Nano Today 43 (2022) 101416.
[53] M. Peng, F. Chen, Z. Wu, J. Shen, Front. Microbiol. 12 (2021) 670874.
[54] T. Verfaillie, A.D. Garg, P. Agostinis, Cancer Lett. 332 (2013) 249–264.
[55] P.M. George, A.U. Wells, R.G. Jenkins, Lancet Respir. Med. 8 (2020) 807–815.
[56] A.C. McKown, E.M. McGuinn, L.B. Ware, L. Wang, D.R. Janz, T.W. Rice, M.W. Semler, Crit. care Med. 45 (2017) 774–780.
[57] G.U. Meduri, W. Bell, S. Sinclair, D.J.L.P.M. Annane, 40 (2011) e543–e560.
[58] G.U. Meduri, D. Annane, M. Confalonieri, G.P. Chrousos, B. Rochwerg, A. Busby, B. Ruaro, B. Meibohm, Intensive Care Med 46 (2020) 2284–2296.
[59] A.T. Bender, C.L. Ostenson, D. Giordano, J.A. Beavo, Cell. Signal. 16 (2004) 365–374.